Translation control by maternal Nanog promotes oocyte maturation and early embryonic development

Mudan He[1,2&], Shengbo Jiao[1,2&], Ding Ye[1,2], Houpeng Wang[1,2], Yonghua Sun[1,2,3*]

[1]State Key Laboratory of Freshwater Ecology and Biotechnology, Institute of Hydrobiology, Innovation Academy for Seed Design, Chinese Academy of Sciences, Wuhan 430072, China

[2]College of Advanced Agricultural Sciences, University of Chinese Academy of Sciences, Beijing 100049, China

[3]Hubei Hongshan Laboratory, Wuhan 430070, China

[&]These authors contributed equally to this work

*Correspondence: yhsun@ihb.ac.cn

Key words: translation control, oocyte maturation, Nanog, zebrafish, embryogenesis

Abstract

Many maternal mRNAs are translationally repressed during oocyte maturation and spatio-temporally activated during early embryogenesis, which is critical for oocyte and early embryo development. By analyzing maternal mutants of *nanog* (M*nanog*) in zebrafish, we demonstrated that Nanog tightly controls translation of maternal mRNA during oocyte maturation via transcriptional repression of *eukaryotic translation elongation factor 1 alpha 1, like 2* (*eef1a1l2*). Loss of maternal Nanog led to defects of egg maturation, increased endoplasmic reticulum (ER) stress, and an activated unfold protein response (UPR), which was caused by elevated translational activity. We further demonstrated that Nanog, as a transcriptional repressor, represses the transcription of *eefl1a1l2* by directly binding to the *eef1a1l2* promoter during oocyte maturation. More importantly, depletion of *eef1a1l2* in *nanog* mutant females effectively rescued the elevated translational activity in oocytes, egg quality defects, and embryonic defects of M*nanog* embryos. Thus, our study demonstrates that maternal Nanog regulates oocyte maturation and early embryogenesis though translational control of maternal mRNA via a novel mechanism, in which Nanog acts as a transcriptional repressor to suppress transcription of *eef1a1l2*.

Introduction

During oocyte development, lots of maternal mRNAs are transcribed and accumulated, and translational activation or repression of maternal mRNA in temporal and spatial determines oocyte development, maturation, and early embryogenesis. Translation of many maternal mRNAs is repressed during oocyte development (Evans and Hunter, 2005; Pique et al., 2008; Gosden and Lee, 2010), and maintenance of translational arrest of maternal mRNA is essential for normal oocyte development and maturation (Richter and Lasko, 2011; Yarunin et al., 2011). Failure of translational repression of maternal mRNAs resulted in various developmental defects, including apoptosis of oogenesis, impaired oocyte maturation and unsuccessful early embryonic development.

Various mechanisms of translational control have been described using different animal models. In zebrafish, the RNA-binding protein Zar1 binds to zona pellucida (ZP) mRNAs and represses translation of the ZP gene during oogenesis, loss of Zar1 induces oocyte apoptosis and ovary degeneration (Miao et al., 2017). An RNA-binding protein Ybx1 associates with processing body components and repress global translation activity during early embryogenesis (Sun et al., 2018). In *Drosophila*, translation of many germ cell-specific mRNAs are repressed by RNA-binding proteins during oocyte maturation. Germline RNA, *oskar* and *pgc*, are targeted by Bruno or Pumilio at the 3'-untranslated region (UTR) and translationally repressed during

oogenesis, and mutation of RNA-binding sites results in precocious translation and mislocalization of mRNA (Kim-Ha et al., 1995; Snee et al., 2008; Flora et al., 2018). Me31B mediates the translational silencing of both maternal mRNAs during the maternal-to-zygotic transition (MZT) and oocyte-localizing RNAs in the transport process to oocyte (Nakamura et al., 2001; Wang et al., 2017). During the transport of *nanos* mRNA to oocyte, the failure of translational repression of *nanos* mRNA by Smaug would lead to ectopic translation of *nanos* and defects of anteroposterior axis formation (Dahanukar and Wharton, 1996; Smibert et al., 1996; Smibert et al., 1999). To date, the studies of translational repression in oogenesis have focused mainly on the posttranscriptional regulation, in which the translational repressors are mainly RNA-binding proteins. It remains elusive whether there is a general translational repressor that regulates the translation of maternal mRNAs at a global level in oocytes.

Nanog is known for its prominent function as a regulator of pluripotency in embryonic stem cells (Mitsui et al., 2003; Boyer et al., 2005; Loh et al., 2006) and reprogramming of somatic cells to the pluripotent state (Takahashi and Yamanaka, 2006; Silva et al., 2009). In zebrafish, Nanog has been shown to be a transcriptional activator to play a central role in regulating early embryogenesis. For instance, maternal Nanog mediates endoderm formation through the Mxtx2-Nodal signaling (Xu et al., 2012), and is required for both extra-embryonic development (Gagnon et al., 2017) and embryonic

architecture formation (Veil et al., 2018). During the maternal-to-zygotic transition (MZT), the maternally provided transcription factors, Pou5f3, SoxB1, and Nanog coordinately open up chromatin to initiate zygotic genes activation (Lee et al., 2013; Veil et al., 2019; Palfy et al., 2020). Our recent study shows that Nanog represses the global activation of maternal β-catenin activity to safeguard the dorsal-ventral axis formation (He et al., 2020). However, as a strongly maternally expressed gene, the role of Nanog in oocyte development and maturation is still unknown.

In this study, we found that the absence of maternal *nanog* led to various developmental defects in oocytes and early embryos. Our study demonstrates the global translational activity is greatly enhanced in *nanog* mutant oocytes and maternal *nanog* mutant (M*nanog*) embryos, due to the transcriptional activation of *eukaryotic translation elongation factor 1 alpha 1, like 2* (*eef1a1l2*) during oocyte maturation. We further show that maternal depletion of *eef1a1l2* significantly rescues the developmental defects of *nanog* mutant oocytes and early development of M*nanog* embryos. Thus, our study reveals a novel role for zebrafish Nanog as a general translational repressor through transcriptional repression of *eef1a1l2* in oocyte maturation.

Results

Maternal *nanog* is required for oocyte maturation and early embryonic development

We have obtained *nanog* mutant using TALEN technology and addressed its critical role in regulating dorsal formation through interfering with TCF factors in previous studies (He et al., 2015; He et al., 2020). Through analyzing the phenotype of M*nanog* embryos, we found that the M*nanog* embryos showed slow epibolic movement, resulting in the accumulation of blastomere cells at the animal pole at gastrulation stage (Fig. 1A), which is similar to the phenotype of maternal and zygotic mutant of *nanog* (MZ*nanog*) (He et al., 2020). Comparing the size of M*nanog* and WT embryos at 15 minutes post fertilization (mpf), the M*nanog* embryos showed significantly shorter chorion diameter and oocyte diameter than WT embryos (Fig. 1B-D). In addition, we analyzed the activation phenotype of mutant egg by monitoring the cortical granule (CG) exocytosis and cytoplasmic streaming. Fluorescein-conjugated *Maclura pomifera* lectin was used to label CGs to assess CG exocytosis in activated eggs. Compared with WT eggs, *nanog* mutant eggs showed abundantly retained CGs (Fig. 1E) at 10 minutes post activation (mpa). CellTracker™ CM-DiI Dye was injected into the yolk of M*nanog* and WT embryo to monitor cytoplasmic streaming. In WT embryos, vigorous cytoplasmic movement toward the animal pole was recorded (Movie 1). In contrast, M*nanog* embryos showed sluggish cytoplasmic streaming (Movie 2).

These results indicate that maternal Nanog is essential for egg activation and early embryonic development.

Moreover, the TUNEL assay showed apoptotic signals appeared in Balbiani bodies and the cytoplasm of early-stage mutant oocytes, but not in WT oocytes (Fig. S1A). Mitochondria are enriched in the Balbiani body and also present throughout the oocyte cytoplasm (Marlow and Mullins, 2008; Jamieson-Lucy and Mullins, 2019), thus *nanog* deficiency induced the mitochondrial apoptosis during oocyte maturation. Besides, robust active-Caspase3 signals was also detected in M*nanog* embryos but not WT embryos at 75% epiboly stage (Fig. S1B). These data demonstrate *nanog* depletion induces the oocyte apoptosis and the death of early embryonic cells.

Through morphological and histological analyses, we found the gonadosomatic index (GSI; gonad weight/body weight X 100%) was significantly reduced in *nanog*$^{-/-}$ compared to WT females (Fig. 1F, G), indicating defects of oocyte maturation in *nanog* mutants. To furtherly characterize the defects of oocyte maturation of *nanog* mutant, stage IV oocytes were isolated and treated with 17α,20β-dihydroxy-4-pregnen-3-one (DHP) to determine the percentage of germinal vesicle breakdown (GVBD) *in vitro.* After 2 hours incubation, the percentage of GVBD in *nanog* mutant oocytes is 15.5%, which is significantly lower than that in WT oocytes (72.4%) (Fig. 1H, I). Moreover, the *nanog* mutant stage V oocyte showed less transparent than WT (Fig. 1J). During the oocyte maturation, the major yolk

proteins undergo cleavage and change the appearance of oocyte from opaque to transparent (Dosch et al., 2004). So we compared the composition of the higher and lower molecular weight yolk proteins (HYP and LYP) from stage III to stage V oocytes, to evaluate the yolk protein cleavage level. In stage III oocytes, the HYP/LYP ratio were even lower in *nanog* mutant than in WT, whereas the ratio was greatly decreased in WT stage V oocytes than in mutants (Fig. 1K). These results suggested the deficiency of yolk protein cleavage during maturation of *nanog* mutant oocytes. In addition, we also generated a transgenic line of *Tg(CMV:nanog-myc*) in *nanog* homozygous background. Immunofluorescence staining showed Nanog is strongly expressed in early oocytes using anti-Myc antibody (Fig. S1C). Moreover, this overexpression of *nanog* could rescue the early developmental defects of M*nanog* (Fig. S1D), demonstrating that oocyte maturation defect and early embryonic defect were caused by deficiency of Nanog. Therefore, we conclude that loss of maternal *nanog* leads to pleiotropic defects of oocyte maturation and early embryonic development.

Loss of maternal *nanog* elevates the global translation level

In order to understand the molecular mechanism of Nanog regulating oocyte maturation, we quantitatively compared proteomes of *nanog* mutant eggs with WT using isobaric tags for relative and absolute quantitation (iTRAQ) technology. More than 1600 proteins were identified in eggs from the two

genotypes. The identified proteins were classified using COG database (Clusters of Orthologous Groups of proteins), and two top categories are involved in the protein translation-related biological process (cluster J and O) (Fig. S2A). Compared the mutant with WT, 67 proteins show differential expression (P<0.05) (S1Table), and 39 proteins were increased in mutant eggs (Fig. S2B). Gene ontology analysis of the upregulated proteins showed that one of the most significant enriched biological processes is translation elongation factor activity (Fig. S2C). Gene-Concept Network showed four elongation factors were enriched (Fig. S2D). These results imply that the global translation activity is elevated in *nanog* deficiency eggs.

To verify this speculation, we assessed the translation activity of M*nanog* embryos at early developmental stage. The mCherry reporter mRNA was injected into one-cell stage WT and M*nanog* embryos together with the same amount of GFP protein. The injected embryos were imaged under a fluorescence microscope at later stages and fluorescence levels were measured. The GFP protein acted as the loading control for injection. Fluorescence measurement showed that the reporter mRNA translation level was significantly higher in M*nanog* embryos (Fig. 2A, B). Using western blotting analysis, we confirmed the increase of mCherry reporter translation in maternal *nanog*-depleted embryos (Fig. 2C, D). More interesting is, we treated the stage IV mutant oocytes with an inhibitor of translation initiation factor, *eif4a*, and determined the percentage of GVBD in vitro. After 2 hours

incubation, the percentage of GVBD was remarkably increased from 10.4% to 28.3% in mutant oocytes (Fig. S2E, F). Taken together, these results suggest that Nanog is necessary for repressing the global translation of maternal mRNAs during oocyte maturation and early embryonic development.

Nanog depletion triggers ER stress and the unfolded protein response (UPR)

The endoplasmic reticulum (ER) functions as a crucial machinery for protein synthesis, modification and trafficking in eukaryotic cells. Under ER stress, cells activate the UPR to alleviate ER burden by reducing protein translation, increasing protein degradation and generating additional chaperones to assist protein folding. Therefore, ER stress and the UPR are often associated with aberrant translational derepression (Kaufman, 2002; Miao et al., 2017). The UPR functions through three major pathways, initiated by three ER-localized transmembrane proteins, such as protein kinase RNA-like ER kinase (PERK), activating transcription factor 6 (ATF6), and Inositol-requiring enzyme 1 (IRE1), to maintain ER homeostasis (Hetz, 2012). Normally, the N-terminal of these transmembrane ER proteins are held by ER chaperone Hspa5 (also termed Grp78 or Bip), preventing their aggregation. When misfolded proteins accumulate, Hspa5 releases, allowing aggregation of these transmembrane signaling proteins, and launching the UPR (Rao and Bredesen, 2004; Shen et al., 2004; Schroder and Kaufman, 2005). Activation of PERK upregulates the

expression of CCAAT-enhancer-binding protein homologous protein (CHOP), which induces cell apoptosis and death (Oyadomari and Mori, 2004; Iurlaro and Muñoz-Pinedo, 2016). We detected the transcriptional level and protein level of *hspa5* and CHOP-encoding gene *ddit3* in mutant ovary, found that both transcription and translation of *hspa5* and *ddit3* are increased in *nanog*$^{-/-}$ ovary (Fig. 2, E-G). TUNEL assay also showed obvious apoptosis signal in mutant ovary (Fig. S1A). Due to lack of specific antibodies against zebrafish ATF6 and IRE1A, we detected the mRNA expression of *atf6* and *ire1a*, and discovered that both of *atf6* and *ire1a* expression were increased in mutant oocytes (Fig. 2H, I). Since phosphorylated ribosomal protein S6 (pS6) is considered an indicator of active protein synthesis (Biever et al., 2015; Meyuhas, 2015), we also detected the expression level of total S6 and pS6, and found that the pS6 level was significantly increased in *nanog* mutant ovary (Fig. 2J, K). Finally, we used PERK inhibitors (GSK2606414 and ISRIB) to treat *nanog* mutant oocytes and determined the occurrence of GVBD. In both treatments, the percentage of GVBD of mutant oocytes were recovered (Fig. 2L, M). These results demonstrate that loss of *nanog* triggers ER stress and UPR and thus leads to failure of oocyte maturation.

Loss of maternal Nanog up-regulates *eef1a1l2* transcription level

To find out the molecular mechanism responsible for Nanog regulating translation activity in early embryos, we conducted RNA sequencing (RNA-seq)

analysis between *nanog* mutant eggs and WT eggs (accession number: PRJNA633216). A total of 207 genes are differentially expressed between mutant and WT eggs, with 102 upregulated genes and 105 downregulated genes in mutant eggs. Among the upregulated genes, the difference of *eukaryotic elongation factor 1 alpha 1, like 2* (*eef1a1l2*) is among the most significant ones (Fig. 3A). The eEF1A1l2 is a major subunit of the translation elongation factor 1 complex (eEF1), which plays a central role in protein synthesis by delivering aminoacyl-tRNAs to the elongating ribosome (Sasikumar et al., 2012). RPKM calculation and visualization of RNA-seq reads mapped to the *eef1a1l2* showed significant upregulation of *eef1a1l2* in mutant eggs (Fig. S3A, B). Reverse-transcription quantitative PCR (RT-qPCR) further proved that the transcription of *eef1a1l2* was significantly increased in *nanog* mutant oocytes at five different stages and in early embryonic developmental stages (Fig. 3B, S3C). In situ hybridization of ovary cryosection also showed increased expression of *eef1a1l2* in *nanog* mutant (Fig. 3C). In contrast, transgenic overexpression of *nanog* significantly decreased the high expression levels of *eef1a1l2* in mutant oocytes (Fig. 3B, C). These data indicate that *nanog* deficiency led to strong transcriptional activation of *eef1a1l2* during oocyte maturation.

To verify the transcriptional inhibition of *eef1a1l2* by Nanog, wildtype *nanog* or a constitutive repressor type *nanog* (Engrailed fusion with Nanog homeodomain, En-*nanog*) (He et al., 2020) was overexpressed and the

transcription of *eef1a1l2* was measured at shield stage. Both in situ hybridization and RT-qPCR analysis showed that the expression of *eef1a1l2* was significantly reduced in both *nanog* and En-*nanog* overexpressed-embryos (Fig. 3D, E), suggesting that Nanog acts as a transcriptional repressor on the regulation of *eef1al2*. To clarify whether Nanog directly bind to the promoter region of *eef1a1l2* to repress its transcription, a chromatin immunoprecipitation (ChIP) assay was conducted. Ovaries of *Tg*(CMV:*nanog-myc*) at 6mpf were dissected and ChIP was performed using anti-Myc antibody. The precipitated chromatin was then analyzed by PCR using primer pairs that could amplify fragments of *eef1a1l2* promoter. A fragment of the *rpl5b* exon amplified by a specific primer pair was used as control (Belting et al., 2011). As shown in Fig. 3F, promoter fragment of *eef1a1l2* was significantly enriched in the immunoprecipitated while no enrichment of the control genomic region *rpl5*. Thus, this result demonstrates that Nanog directly binds to the promoter of *eef1a1l2* to inhibit its transcription. All these data illustrate that Nanog directly inhibits the transcription of *eef1a1l2* and depletion of *nanog* leads to significantly increased expression of *eef1a1l2*.

Deficiency of eEF1A1l2 ameliorates impaired oocyte maturation of *nanog* mutants

We then generated homozygous mutant of *eef1a1l2* and two types of *eef1a1l2* mutants were obtained and neither of them showed obvious defect (Fig. S4),

and we used the ihb99 allele for subsequent study. To determine if Nanog promotes oocyte maturation through suppression of *eef1a1l2*, we generated double homozygous mutant of *nanog* and *eef1a1l2* and studied whether depletion of *eef1a1l2* could ameliorate the oocyte maturation defect of *nanog* mutant. Through morphological analysis, we found double maternal mutant (M*nanog*, M*eef1a1l2*) showed increased embryo chorion diameter and oocyte diameter at 15 mpf, compared to M*nanog* embryos (Fig. 4A-C). The process of cortical granule (CG) exocytosis in double mutant eggs (*nanog*,*eef1a1l2*) were also comparable to WT at 10 mpa, which showed less retained CGs than *nanog* mutant (Fig. 4D). Moreover, cytoplasmic streaming labeled by CM-DiI Dye in double maternal mutant embryo (M*nanog*, M*eef1a1l2*) showed vigorous cytoplasmic movement, similar to the WT (Movie 3). These results indicate that depletion of *eef1a1l2* rescues the egg activation defect of *nanog* mutant.

Therefore, we further examined the oocyte maturation improvement in double mutant. Morphologically, The GSI was increased in double mutant (*nanog*$^{-/-}$, *eef1a1l2*$^{-/-}$) female, compared to *nanog*$^{-/-}$ (Fig. 4E, F). The double mutant eggs showed more transparent than *nanog* mutant, similar to WT (Fig. 4G). The altered ratio of the higher and lower molecular weight yolk proteins (HYP and LYP) from stage III oocytes to stage V oocytes in double mutant confirmed this conclusion (Fig. 4H). The % GVBD was also remarkably increased in double mutant oocytes (Fig. 4I, J). These results together indicate

that Nanog promotes oocyte maturation through suppressing the expression of *eef1a1l2* in oocyte.

Depletion of *eef1a1l2* alleviates the ER stress and UPR in *nanog* mutant oocyte

Since depletion of *eef1a1l2* could ameliorates the oocyte maturation defect of *nanog* mutant, we wondered the eEF1A1l2 depletion on alleviating of ER stress. We addressed the mRNA expression level of ER stress-associated genes, found that the increased expression of *hspa5*, *ddit3*, *atf6* and *ire1a* in *nanog* mutant ovary were all restored in *nanog* and *eef1a1l2* double mutant (Fig. 5A-D). IRE1 is a unique RNase which removes an internal 26 nucleotides from X-box binding protein 1 (XBP1) mRNA transcripts in the cytoplasm and activates gene expression involved in protein folding and degradation, thus the splicing of XBP1 mRNA has been established as a common indicator of ER stress (Shen et al., 2001; Yoshida et al., 2001; Li et al., 2015). We detected the altered splicing of *xbp1* in ovary of mutant and WT, discovered the splicing ratio of *xbp1* was increased in *nanog* mutant ovary, and this excessive splicing was reduced in double mutant ovary (Fig. 5E, F).

To observe organelle changes that may accompany response to ER stress, ultrastructure analysis using transmission electron microscopy (TEM) was performed in stage I oocytes of WT, *nanog* mutant, and double mutant. The WT oocytes showed normal morphology of ER, Golgi apparatus and

mitochondria (Fig. 5G, a and d). However, *nanog* mutant oocytes showed disruption of Golgi apparatus, including swelling of Golgi apparatus, dilated and disintegrated vesicles, and collapse of Golgi complex (Fig. 5G, b, white arrowheads). *nanog* mutant oocytes also showed incompact and swollen mitochondria (Fig. 5G, e, yellow arrowheads), as well as evident lysosome distribution (Figure 5G, e, red arrowheads). In contrast, *nanog* and *eef1a1l2* double mutant showed well structure of ER, Golgi apparatus and mitochondria (Figure 5G, c, f). These data demonstrate that depletion of *eef1a1l2* alleviates the ER stress and UPR in *nanog* mutant, indicating that transcriptional activation of *eef1a1l2* in *nanog* mutant oocytes inducing ER stress and UPR, thus leading to defects of oocyte maturation.

Depletion of *eef1a1l2* rescues early embryonic development defect of *nanog* mutant

Given that depletion of *eef1a1l2* could rescue the oocyte maturation defect and alleviate the ER stress/UPR, we wondered the rescue effect of depletion of *eef1a1l2* on early embryonic development defect. Due to the translation elongation role of eEF1A1l2, we firstly assessed the translation level of double mutant. mCherry mRNA reporter and GFP protein were co-injected at one-cell stage in WT, M*nanog*, and M*nanog*,M*eef1a1l2* embryos. Fluorescence intensity of mCherry was measured at 4 hpf. Fluorescence measurement showed that the reporter translation level was significantly reduced in

343 M*nanog*,M*eef1a1l2* embryos (Fig. S5A, B), suggesting the elevated translation
344 level of *nanog* mutant was decreased by depletion of *eef1a1l2*.

345 Next, we examined the early embryonic development phenotype of double
346 mutant. The morphological phenotypes of WT, M*nanog* (*nanog*$^{-/-}$ female cross
347 with WT male), M*nanog*,M*eef1a1l2* (*nanog*$^{-/-}$,*eef1a1l2*$^{-/-}$ female cross with WT
348 male), M*nanog*,MZ*eef1a1l2* (*nanog*$^{-/-}$,*eef1a1l2*$^{-/-}$ female cross with *eef1a1l2*$^{-/-}$
349 male), and M*nanog*,Z*eef1a1l2* (*nanog*$^{-/-}$,*eef1a1l2*$^{+/-}$ female cross with
350 *eef1a1l2*$^{-/-}$ male and *nanog*$^{+/-}$,*eef1a1l2*$^{-/-}$ embryos were genotyped) were
351 recorded at 0.2, 8, 12 and 24 hpf, respectively. As described in Fig. 1A,
352 blastomere cells stacked at the animal pole and unable to complete the
353 gastrulation in M*nanog* embryos. Until 24 hpf, M*nanog* embryos still showed
354 abnormal shapes and died gradually (Fig. 6A). Surprisingly, either getting rid of
355 maternal increased *eef1a1l2* in M*nanog*,M*eef1a1l2* embryos, or eliminating
356 both maternal and zygotic increased *eef1a1l2* in M*nanog*,MZ*eef1a1l2* embryos,
357 could effectively rescue the developmental defects of M*nanog* (Fig. 6A).
358 M*nanog*,M*eef1a1l2* and M*nanog*,MZ*eef1a1l2* embryos both exhibited
359 ameliorated epiboly movement at gastrulation stage and improved axial
360 formation excepting telencephalon defect at prim-stage. However,
361 M*nanog*,Z*eef1a1l2* embryos only lacking the zygotic *eef1a1l2* exhibited similar
362 phenotype with M*nanog* (Fig. 6A), indicating that the maternally provided
363 *eef1a1l2* mRNA in M*nanog*,Z*eef1a1l2* still led to developmental failure. In
364 summary, only if *eef1a1l2* was completely disrupted in the *nanog* mutant

oocytes, the M*nanog*,M*eef1a1l2* or M*nanog*,MZ*eef1a1l2* embryos displayed rescued early embryonic development. These data indicate that support the c maternal activation of *eef1a1l2* in *nanog* mutant oocytes not only leads to oocyte maturation defects, but also results in early developmental defects of M*nanog* embryos.

Furthermore, we investigated the rescue effects using a set of molecular markers representing different functions of Nanog in early development. Several studies have proved that maternal Nanog directly activates *mxtx2* to regulate endoderm and extraembryonic formation through Nanog-*mxtx2*-Nodal pathway (Xu et al., 2012; Gagnon et al., 2018; Veil et al., 2018).We confirmed that the expression of *mxtx2* was absent in M*nanog*, while the disappearance of *mxtx2* transcripts could be restored in M*nanog*,M*eef1a1l2* (Fig. 6B, S5C). During zebrafish zygotic genome activation (ZGA), together with Pou5f3 and SoxB1, maternal Nanog initiates the transcription of the first major wave of zygotic genes and directly activates microRNA miR-430, maternal mRNAs were then cleared by miR-430 at the post-ZGA (Giraldez et al., 2006; Lee et al., 2013). The expression of zygotic genes, miR-430 and *blf*, failed to be activated, and maternal mRNA *sod1*, which is targeted by miR-430, also failed to be removed at post-ZGA in M*nanog* (Fig. 6B, S5D-F). In contrast to rescue of *mxtx2* expression, the defects of ZGA and maternal mRNA clearance could not be rescued in M*nanog*,M*eef1a1l2* embryos (Fig. 6B, S5D-F). These results illustrate that during oogenesis, maternal Nanog safeguards the oocyte

maturation by suppression the transcriptional activation of *eef1a1l2* as a transcriptional repressor, and during early embryogenesis, the transcriptional suppression of *eef1a1l2* by Nanog is mainly required for transcription initiation of *mxtx2* and YSL formation.

All these results deciphered a following molecular picture: during oocyte maturation and early embryogenesis (Fig. 6C). During WT oogenesis, Nanog acts as a transcriptional repressor, with certain co-repressors, directly inhibits the transcription of eukaryotic translation elongation factor, *eef1a1l2*, contributing to the translational control in oocytes. After fertilization, Nanog acts as a transcriptional activator, together with Pou5f3 and SoxB1, to initiate zygotic genome activation. In the oocytes produced by *nanog*$^{-/-}$ females, the transcriptional inhibition of *eef1a1l2* is absent, ectopic maternal proteins are translated and accumulated, thus inducing ER stress and excessive UPR, and leading to oocyte maturation defects. The embryos fertilized from the *nanog*$^{-/-}$ defective eggs failed to undergo normal gastrulation. In the oocytes produced by *nanog*$^{-/-}$,*eef1a1l2*$^{-/-}$ females, however, the translation level of maternal mRNAs is mitigated owing to the lack of functional eEF1A1l2, and ER stress and UPR are alleviated, therefore leading to a normal oocyte maturation. Therefore, it is likely that Nanog shifts from a transcriptional repressor to a transcription activator during oocyte-to-zygote transition (OZT), which are both essential for early embryogenesis.

Discussion

The function of Nanog at early embryonic developmental stages has been well characterized in previous studies(Veil et al., 2018; Veil et al., 2019; He et al., 2020; Palfy et al., 2020). However, as a maternal expressed gene, its role in oocyte development and maturation is still unknown. In this study, we revealed that zebrafish Nanog is essential for oocyte maturation, which function has a lasting effect on early embryogenesis. Loss of maternal Nanog causes impaired oocyte maturation, deficient egg activation, and early embryo developmental failure. Impaired oocyte maturation correspondingly tends to produce poor-quality egg. We have compared the *nanog* expression level in good-quality egg and poor-quality egg and found that *nanog* expression is significantly decreased in poor-quality egg (Fig. S6), suggesting that Nanog might be a new factor for oocyte quality assessment. Mechanistically, Nanog transcriptionally represses the expression of translation elongation factor *eef1a1l2* to maintain a translational control state during oocyte maturation. In contrast, in *nanog* mutant oocytes, ectopic transcriptional activation of *eef1a1l2* elevates global translation activity and causes ER stress and UPR. Depletion of *eef1a1l2* could rescue the oocyte maturation defects and embryonic defects of *nanog* mutant. Taken together, our results delineate the mechanisms underlying a general translation repressor role of Nanog during oocyte maturation.

Maternal mRNAs synthesized in oocyte initiate the development of future

generations. Some maternal mRNAs are either somatic or germline determinants and must be translationally repressed until embryogenesis (Richter and Lasko, 2011; Flora et al., 2018). Previous studies have provided numerous examples of how sequence-specific regulators, mostly RNA-binding proteins, maintain translational repression levels of mRNAs containing targeted cis-regulatory elements post-transcriptionally in gametogenesis and early embryogenesis (Kugler and Lasko, 2009; Kotani et al., 2013; Winata et al., 2017; Sun et al., 2018). In this study, we showed a transcriptional factor, Nanog, transcriptionally inhibits the expression of a translation elongation factor, eEF1A1l2 consequently controls the global mRNA translation activity during oocyte maturation. This translation repressive manner is realized through regulating the activity of a translation machinery, which is more global and independent on the sequence specificity of mRNA. Thus, this study revealed a novel translational control mechanism regulated by Nanog to promote oocyte maturation and early embryogenesis.

The genes who are not transcribed in oocyte and maturate eggs are considered as non-maternal genes, or zygotic genes. In theory, the transcription of non-maternal genes should be suppressed in oocyte to safeguard the oocyte maturation and early embryo patterning. The abnormal activation and expression of non-maternal genes will change the oocyte cell fate, affect egg quality, even lead to the apoptosis of oocyte. According to the expression pattern of *eef1a1l2* addressed during oocyte maturation and early

453 embryonic development in WT (Fig. 3, S4), we found that *eef1a1l2* has no
454 maternal expression in oocytes, indicating *eef1a1l2* is a non-maternal gene
455 and not employed during oocyte maturation. However, *eef1a1l2* is
456 precociously transcribed in *nanog* mutant oocytes, which leads to the
457 over-activation of global translation activity, further results in the impaired
458 oocyte maturation. This finding implies us Nanog safeguards oocyte
459 maturation and early embryogenesis possibly by suppression the
460 transcriptional activation of non-maternal genes.

461 Studies in human and mouse embryonic stem cells (ESC) revealed Nanog
462 acts as both transcriptional activator and transcriptional repressor (Boyer et al.,
463 2005; Liang et al., 2008). As a transcriptional activator, Nanog cooperating with
464 Pou5f3 and Sox2, transcriptionally activates the expression of genes
465 responsible for stem cell self-renew and pluripotency maintenance, while as a
466 transcriptional repressor, Nanog associates with repression complexes and
467 transcriptionally represses the expression of genes related to differentiation
468 and development. In this study, we concluded that Nanog acts as a
469 transcriptional repressor to suppress the transcription of *eef1a1l2* and
470 speculated that Nanog safeguards oocyte maturation by suppressing *eef1a1l2*
471 during oocyte development in zebrafish. However, zebrafish Nanog is
472 well-known for acting as a transcription activator in zygotic genome activation
473 (ZGA) and shaping the embryo during gastrulation. For instance, together with
474 Pou5f3 and SoxB1, Nanog initiates the zygotic gene activation (ZGA), of which

475 miR-430 is directly activated by Nanog and responsible for clearance of
476 maternal mRNA during MZT (Lee et al., 2013). Further studies proved Nanog
477 binds to the high nucleosome affinity regions (HNARs) center and opens
478 chromatin with Pou5f3 and Sox19b synergistically, primes genes for activity
479 during ZGA in zebrafish (Veil et al., 2019; Palfy et al., 2020). Nanog directly
480 activates *mxtx2* and regulates the extraembryonic tissue and and embryonic
481 architecture formation (Xu et al., 2012; Gagnon et al., 2018; Veil et al., 2018).
482 Quantitative imaging also reveals Nanog cooperates with Pou5f3 to promote
483 ventral fate (Perez-Camps et al., 2016). These studies illustrate that Nanog
484 switches from transcriptional repressor to transcriptional activator during
485 oocyte-to-zygote transition. As a homeodomain protein, Nanog binds with
486 target genes at homeobox domain, while which repressive partner interacts
487 with Nanog to exhibit gene silence function in oocyte still needs to be further
488 investigated.
489

Methods and Materials

Zebrafish maintenance

All the zebrafish used in this study were maintained and raised as previously described (Westerfield, 1995) at the China Zebrafish Resource Center of the National Aquatic Biological Resource Center (CZRC-NABRC, Wuhan, China, http://zfish.cn). The Wildtype (WT) embryos were collected by natural spawning from AB strain. Oocyte developmental stages were classified according to previous studies (Selman et al., 1993; Lubzens et al., 2010). Developmental stages of mutant embryos were indirectly determined by observation of WT embryos born at the same time and incubated under identical conditions. The experiments involving zebrafish were performed under the approval of the Institutional Animal Care and Use Committee of the Institute of Hydrobiology, Chinese Academy of Sciences under protocol number IHB2014-006.

Double mutant generation of *nanog* and *eef1a1l2*

M*nanog* was generated by crossing *nanog*$^{-/-}$ female with WT male as previously described (He et al., 2015; He et al., 2020). *eef1a1l2* mutant was generated in *nanog* mutant background using CRISPR/Cas9. The gRNA target and PAM sequence (underlined) of *eef1a1l2* is 5'-GGCCACCTCATTTACAGTGTGG-3', pT3TS-zCas9 was used for Cas9 mRNA transcription; capped Cas9 mRNA was generated using T3 mMessage

Machine kit (AM1344, Ambion). gRNA was generated using in vitro transcription by T7 RNA polymerase (Promega, USA). Cas9 mRNA and gRNA were co-injected into embryos crossed by *nanog*$^{+/-}$ female and *nanog*$^{-/-}$ male at one-cell stage. M*nanog*/M*eef1a1l2* was obtained by crossing *nanog*$^{-/-}$,*eef1a1l2*$^{-/-}$ female with WT male. The primers used for mutant screening are listed in S2 Table.

Morphological analysis of ovary and oocyte

After MS-222 anesthesia, we dissected the intact gonadal tissues from WT, *nanog*$^{-/-}$, and *nanog*$^{-/-}$,*eef1a1l2*$^{-/-}$ adult zebrafish (4-months post fertilization) and calculated the gonadosomatic index (GSI; gonad weight/body weight X 100%). For embryos, chorion elevation distance and oocyte diameter were measured at 15 minute-post-fertilization (mpf) using ImageJ. Oocyte diameter was the longest distance in the vertical direction of the animal-vegetal axis. Chorion diameter was the longest length of chorion when it was fully inflated.

Oocyte isolation, in vitro culture and germinal vesicle breakdown (GVBD) assay

Ovaries were dissected from adult females and transferred into oocyte sorting medium (OSM), made from 90% Leibovitz's L-15 medium (Gibco, USA) and 10% Fetal Bovine Serum (BI, Israel) with 100μg/ml Penicillin-Streptomycin (Gibco, USA). Oocytes were manually separated and divided into five groups

based on their size and vitellogenic state: primary growth stage (stage I), previtellogenic stage (stage II), vitellogenic stage (stage III), full-growth stage (stage IV) and the oocyte after GVBD in vitro was defined as stage V (mature oocyte). Ovulated maturation oocyte was defined as egg. Different stages of oocytes were gently separated using two tweezers in a dish covered with 1% agarose.

Dissociated stage IV oocytes were transferred into oocyte culture medium (OCM) by gentle pipetting. OCM was made from 90% Leibovitz's L-15 medium and 10% Fetal Bovine Serum with 1 μg/mL 17α-20β-dihydroxy-4pregnen-3-one (DHP, Cayman, USA). Sorted oocytes were cultured at 28°C for 2h according to previous study (Nair et al., 2013). The GVBD rates were determined in a unified standard by ImageJ. The concentrations of different inhibitors added to OCM were *eif4a* inhibitor (25ng/μL, SantaCruz, USA), ISRIB (5μM, Selleck, Shanghai), GSK2606414 (50nM, Selleck, Shanghai).

Cortical Granules (CGs) staining

Ovulated eggs at 10 minute-post-activation (mpa) in water were collected and fixed with 4% paraformaldehyde (PFA) overnight for further steps. Cortical granules were visualized by staining embryos with 50 μg/ml FITC-conjugated *Maclura pomifera* agglutinin (Vector Laboratories, FL-1341) as previously described (Mei et al., 2009).

556

557 **SDS-PAGE and Coomassie staining**

558 SDS-PAGE and Coomassie staining were performed following the established
559 protocol (Schagger, 2006). To obtain yolk protein, 10 oocytes were cleaved in
560 500 μL TNE buffer, made from 10 mM Tris-HCl (pH=7.4), 150 mM NaCl, 5 mM
561 EDTA and 1% Triton X-100. 10 μL lysate was loaded for SDS-PAGE and
562 Coomassie staining as previously described (Sun et al., 2018). Intensity
563 measurement was done using ImageJ.

564

565 **Western blot analysis**

566 GFP protein was purchased form DIA-AN Biotechnology and 20 pg of GFP
567 protein per embryo was co-injected at one-cell stage. Injected embryos or
568 dissected ovaries were homogenized using RIPA (P0013B, Beyotime).
569 Western blot was carried out as previously described (Ye et al., 2019). Primary
570 antibodies and dilutions for western blot were GAPDH (2058, DIA-AN, 1:3,000),
571 mCherry (BE2026, Easybio, 1:2,000), GFP (2057, DIA-AN, 1:2,000), Hspa5
572 (11587-1-AP, Proteintech, 1:2,000), Ddit3 (AC532, Beyotime, 1:2,000), S6
573 (2217S, CST, 1:1,000), pS6 (2215S, CST, 1:1,000).

574

575 **RNA-seq and analysis**

576 Total RNA of ovulated eggs of WT and *nanog* homozygous were extracted
577 using TRIzol Reagent (Invitrogen) and mRNA was enriched using oligo-dT

magnetic beads. First-strand cDNAs (from purified mRNA) was synthesized using random hexamers. The PCR-amplified cDNA was purified using AMPure XP beads, then 1 μL cDNA was validated using an Agilent 2100 Bioanalyzer. Sequencing libraries were generated using the Illumina TruSeq RNA sample preparation kit v2 according to the manufacturer's recommendations. Clustered library preparations were sequenced on an Illumina HiSeq™ 2000 machine and 100 bp single-end reads were generated. Clean reads, with low quality reads removed from the raw data, were mapped to the zebrafish GRCz10 reference genome using TopHat2 (Kim et al., 2013). HTSeq v0.6.1 was used to count the read numbers mapped to each gene. Then, the RPKM of each gene was calculated to determine gene expression levels (Trapnell et al., 2010). Differential expression analysis was performed using the DESeq (Anders and Huber, 2010). Genes with an adjusted P-value < 0.05 as calculated by DESeq were considered differentially expressed. The original RNA-seq data has been deposited to the BioProject with accession number PRJNA633216.

Proteomics

Ovulated eggs of WT and *nanog* homozygous were pooled and homogenized for quantitative proteomic analysis. The iTRAQ analysis was performed as previously described (Miao et al., 2017). The UniPort proteome sequence for Danio rerio were used for the database searching.

Chromosome-immunoprecipitation PCR (ChIP-PCR)

Chromatin immunoprecipitation (ChIP) assays were performed with a ChIP assay kit (Cell Signaling Technology) as described (Wei et al., 2014). Briefly, 2 ovaries of *Tg*(CMV:*nanog-myc*) at 6mpf were dissected and lysed for ChIP assay. Immunoprecipitation was carried out using anti-Myc antibody (CST). The immunoprecipitation of *eef1a1l2* genomic in immunoprecipitated chromatin was detected by PCR. primers specific for the *eef1a1l2* promoter region were used and the sequences were listed in S2 Table. The exon of ribosomal protein *rpl5b* was served as a negative control, and the primers were 5′-GGGGATGAGTTCAATGTGGAG-3′ (forward) and 5′-CGAACACCTTATTGCCAGTAG-3′ (reverse) as described (Belting et al., 2011).

Transmission electron microscopy (TEM) analysis

Isolated early-stage oocytes from different genotypic ovaries were collected into a test tube and fixed with 100 μL 2.5% glutaraldehyde at 4^{o}C overnight. Samples preparation for transmission electron microscopy (TEM) was according to the previous described (Zhang et al., 2021) and observed under TEM (Hitachi, HT7700).

In situ hybridization

PCR-amplified sequences of genes of interest were used as templates for the synthesis of an antisense RNA probe, labelled with digoxigenin-linked nucleotides. Whole-mount *In situ* hybridization (WISH) on embryos were performed as described previously (Thisse and Thisse, 2008). For *in situ* hybridization on frozen section, adult ovaries were stripped and embedded in Optimal Cutting Temperature compound (O.C.T. SAKURA) and sectioned at 10 μm. The procedures of hybridization followed a previous study (Zhang et al., 2020).

Immunofluorescence

For whole-mount immunofluorescence, embryos were collected and fixed in 4% PFA for overnight at 4^{o}C. For immunofluorescence on cryosections, sections were prepared as in situ hybridization and fixed in 4% PFA for 20 min at room temperature. The procedure of immunostaining on embryos and slides are referred to previous studies, separately (He et al., 2020; Zhang et al., 2021). Primary antibodies and dilutions were Cleaved-Caspase3 (#9661, CST, 1:1,000), Myc (#2276, CST, 1:1,000).

Reverse-transcription quantitative PCR (RT-qPCR)

Total RNA was extracted from indicated samples using TRIzol method. The RNA was reverse-transcribed with PrimeScript™ RT reagent Kit (Thermo) and relative abundance of target mRNAs was examined with gene-specific primers.

644 *gapdh* was used as a normalization control. Sequences of PCR primers are
645 listed in S2 Table. RT-qPCR was performed using the SYBRGreen Super mix
646 from BioRad (USA) on a BioRad CFX96.
647
648 **Stem-loop RT-PCR of miR-430a**
649 Stem-loop RT-PCR was performed to quantify the expression of miR-430a as
650 previously described (Chen et al., 2005). Total RNAs were reversely
651 transcribed using the miR-430a specific primers and U6 was used as internal
652 control. The PCR primers of miR-430a and U6 used in this study referred to
653 previous study (He et al., 2020).
654
655 **Terminal deoxynucleotidyl transferase dUTP nick end labeling (TUNEL)**
656 **assay**
657 Ovaries were dissected from 4 months post fertilization WT and *nanog*$^{-/-}$ adult
658 fish and cryosections were prepared as in situ hybridization. The samples were
659 sectioned at 10 μm thickness. The TUNEL cell death assay was performed
660 using the In Situ Cell Death Detection Kit (Roche) according to the
661 manufacturer's instructions. Images were obtained using a laser scanning
662 confocal microscope (Leica SP8).
663
664 ## Statistical analysis
665 GraphPad Prism 8.3.0 software was used for statistical analyses and statistical

graphs. Significance of differences between means was analyzed using Student's t test. Sample sizes were indicated in the figure legends. Data were shown as mean ± SD. *P* value below 0.05 marked as *, *P* value below 0.01 marked as **, and *P* value below 0.001 marked as ***, ns means no significant difference.

Acknowledgements

We thank other members of the Sun laboratory for discussions, and Linglu Li from the China Zebrafish Resource Center for fish raising assistance.

Competing interests

The authors declare no competing or financial interests.

Funding

This work was supported by National Natural Science Foundation of China under grant No 31702323 to MH, and 31671501 to YS.

Data availability

RNA-seq data in this study have been deposited in SRA under the accession number PRJNA633216. Raw data of the iTRAQ proteome analyses are available in iProX under the accession number IPX0004874000.

References

Anders, S. and Huber, W. (2010) 'Differential expression analysis for sequence count data', *Genome Biol* 11(10): R106.

Belting, Heinz-Georg, Wendik, Björn, Lunde, Karen, Leichsenring, Manuel, Mössner, Rebecca, Driever, Wolfgang and Onichtchouk, Daria (2011) 'Pou5f1 contributes to dorsoventral patterning by positive regulation of vox and modulation of fgf8a expression', *Developmental Biology* 356(2): 323-336.

Biever, A., Valjent, E. and Puighermanal, E. (2015) 'Ribosomal Protein S6 Phosphorylation in the Nervous System: From Regulation to Function', *Front Mol Neurosci* 8: 75.

Boyer, L. A., Lee, T. I., Cole, M. F., Johnstone, S. E., Levine, S. S., Zucker, J. P., Guenther, M. G., Kumar, R. M., Murray, H. L., Jenner, R. G. et al. (2005) 'Core transcriptional regulatory circuitry in human embryonic stem cells', *Cell* 122(6): 947-56.

Chen, C., Ridzon, D. A., Broomer, A. J., Zhou, Z., Lee, D. H., Nguyen, J. T., Barbisin, M., Xu, N. L., Mahuvakar, V. R., Andersen, M. R. et al. (2005) 'Real-time quantification of microRNAs by stem-loop RT-PCR', *Nucleic Acids Res* 33(20): e179.

Dahanukar, A. and Wharton, R. P. (1996) 'The Nanos gradient in Drosophila embryos is generated by translational regulation', *Genes Dev* 10(20): 2610-20.

Dosch, Roland, Wagner, Daniel S., Mintzer, Keith A., Runke, Greg, Wiemelt, Anthony P. and Mullins, Mary C. (2004) 'Maternal Control of Vertebrate Development before the Midblastula Transition: Mutants from the Zebrafish I', *Developmental Cell* 6(6): 771-780.

Evans, T. C. and Hunter, C. P. (2005) 'Translational control of maternal RNAs', *WormBook*: 1-11.

Flora, Pooja, Wong-Deyrup, Siu Wah, Martin, Elliot Todd, Palumbo, Ryan J., Nasrallah, Mohamad, Oligney, Andrew, Blatt, Patrick, Patel, Dhruv, Fuchs, Gabriele and Rangan, Prashanth (2018) 'Sequential Regulation of Maternal mRNAs through a Conserved cis-Acting Element in Their 3′ UTRs', *Cell Rep* 25(13): 3828-3843.e9.

Gagnon, J. A., Obbad, K. and Schier, A. F. (2018) 'The primary role of zebrafish nanog is in extra-embryonic tissue', *Development* 145(1).

Gagnon, James A., Obbad, Kamal and Schier, Alexander F. (2017) 'Zebrafish nanog is

primarily required in extraembryonic tissue', *Development*.

Giraldez, A. J., Mishima, Y., Rihel, J., Grocock, R. J., Van Dongen, S., Inoue, K., Enright, A. J. and Schier, A. F. (2006) 'Zebrafish MiR-430 promotes deadenylation and clearance of maternal mRNAs', *Science* 312(5770): 75-9.

Gosden, Roger and Lee, Bora (2010) 'Portrait of an oocyte: our obscure origin', *Journal of Clinical Investigation* 120(4): 973-983.

He, M. D., Zhang, F. H., Wang, H. L., Wang, H. P., Zhu, Z. Y. and Sun, Y. H. (2015) 'Efficient ligase 3-dependent microhomology-mediated end joining repair of DNA double-strand breaks in zebrafish embryos', *Mutat Res* 780: 86-96.

He, Mudan, Zhang, Ru, Jiao, Shengbo, Zhang, Fenghua, Ye, Ding, Wang, Houpeng and Sun, Yonghua (2020) 'Nanog safeguards early embryogenesis against global activation of maternal β-catenin activity by interfering with TCF factors', *PLOS Biology* 18(7): e3000561.

Hetz, C. (2012) 'The unfolded protein response: controlling cell fate decisions under ER stress and beyond', *Nat Rev Mol Cell Biol* 13(2): 89-102.

Iurlaro, Raffaella and Muñoz-Pinedo, Cristina (2016) 'Cell death induced by endoplasmic reticulum stress', *The FEBS Journal* 283(14): 2640-2652.

Jamieson-Lucy, A. and Mullins, M. C. (2019) 'The vertebrate Balbiani body, germ plasm, and oocyte polarity', *Curr Top Dev Biol* 135: 1-34.

Kaufman, Randal J. (2002) 'Orchestrating the unfolded protein response in health and disease', *The Journal of Clinical Investigation* 110(10): 1389-1398.

Kim-Ha, J., Kerr, K. and Macdonald, P. M. (1995) 'Translational regulation of oskar mRNA by bruno, an ovarian RNA-binding protein, is essential', *Cell* 81(3): 403-12.

Kim, Daehwan, Pertea, Geo, Trapnell, Cole, Pimentel, Harold, Kelley, Ryan and Salzberg, Steven L. (2013) 'TopHat2: accurate alignment of transcriptomes in the presence of insertions, deletions and gene fusions', *Genome biology* 14(4): R36-R36.

Kotani, T., Yasuda, K., Ota, R. and Yamashita, M. (2013) 'Cyclin B1 mRNA translation is temporally controlled through formation and disassembly of RNA granules', *J Cell Biol* 202(7): 1041-55.

Kugler, J. M. and Lasko, P. (2009) 'Localization, anchoring and translational control of oskar, gurken, bicoid and nanos mRNA during Drosophila oogenesis', *Fly (Austin)* 3(1): 15-28.

Lee, M. T., Bonneau, A. R., Takacs, C. M., Bazzini, A. A., DiVito, K. R., Fleming, E. S. and Giraldez, A. J. (2013) 'Nanog, Pou5f1 and SoxB1 activate zygotic gene expression during the maternal-to-zygotic transition', *Nature* 503(7476): 360-4.

Li, Junling, Chen, Zhiliang, Gao, Lian-Yong, Colorni, Angelo, Ucko, Michal, Fang, Shengyun and Du, Shao Jun (2015) 'A transgenic zebrafish model for monitoring xbp1 splicing and endoplasmic reticulum stress in vivo', *Mechanisms of Development* 137: 33-44.

Liang, J., Wan, M., Zhang, Y., Gu, P., Xin, H., Jung, S. Y., Qin, J., Wong, J., Cooney, A. J., Liu, D. et al. (2008) 'Nanog and Oct4 associate with unique transcriptional repression complexes in embryonic stem cells', *Nat Cell Biol* 10(6): 731-9.

Loh, Y. H., Wu, Q., Chew, J. L., Vega, V. B., Zhang, W., Chen, X., Bourque, G., George, J., Leong, B., Liu, J. et al. (2006) 'The Oct4 and Nanog transcription network regulates pluripotency in mouse embryonic stem cells', *Nat Genet* 38(4): 431-40.

Lubzens, E., Young, G., Bobe, J. and Cerda, J. (2010) 'Oogenesis in teleosts: how eggs are formed', *Gen Comp Endocrinol* 165(3): 367-89.

Marlow, F. L. and Mullins, M. C. (2008) 'Bucky ball functions in Balbiani body assembly and animal-vegetal polarity in the oocyte and follicle cell layer in zebrafish', *Dev Biol* 321(1): 40-50.

Mei, W., Lee, K. W., Marlow, F. L., Miller, A. L. and Mullins, M. C. (2009) 'hnRNP I is required to generate the Ca2+ signal that causes egg activation in zebrafish', *Development* 136(17): 3007-17.

Meyuhas, O. (2015) 'Ribosomal Protein S6 Phosphorylation: Four Decades of Research', *Int Rev Cell Mol Biol* 320: 41-73.

Miao, L., Yuan, Y., Cheng, F., Fang, J., Zhou, F., Ma, W., Jiang, Y., Huang, X., Wang, Y., Shan, L. et al. (2017) 'Translation repression by maternal RNA binding protein Zar1 is essential for early oogenesis in zebrafish', *Development* 144(1): 128-138.

Mitsui, K., Tokuzawa, Y., Itoh, H., Segawa, K., Murakami, M., Takahashi, K., Maruyama, M., Maeda, M. and Yamanaka, S. (2003) 'The homeoprotein Nanog is required for maintenance of pluripotency in mouse epiblast and ES cells', *Cell* 113(5): 631-642.

Nair, S., Lindeman, R. E. and Pelegri, F. (2013) 'In vitro oocyte culture-based manipulation of zebrafish maternal genes', *Dev Dyn* 242(1): 44-52.

Nakamura, A., Amikura, R., Hanyu, K. and Kobayashi, S. (2001) 'Me31B silences

translation of oocyte-localizing RNAs through the formation of cytoplasmic RNP complex during Drosophila oogenesis', *Development* 128(17): 3233-42.

Oyadomari, S. and Mori, M. (2004) 'Roles of CHOP/GADD153 in endoplasmic reticulum stress', *Cell Death Differ* 11(4): 381-9.

Palfy, M., Schulze, G., Valen, E. and Vastenhouw, N. L. (2020) 'Chromatin accessibility established by Pou5f3, Sox19b and Nanog primes genes for activity during zebrafish genome activation', *PLoS Genet* 16(1): e1008546.

Perez-Camps, Mireia, Tian, Jing, Chng, Serene C., Sem, Kai Pin, Sudhaharan, Thankiah, Teh, Cathleen, Wachsmuth, Malte, Korzh, Vladimir, Ahmed, Sohail and Reversade, Bruno (2016) Quantitative imaging reveals real-time Pou5f3-Nanog complexes driving dorsoventral mesendoderm patterning in zebrafish *Elife*, vol. 5.

Pique, M., Lopez, J. M., Foissac, S., Guigo, R. and Mendez, R. (2008) 'A combinatorial code for CPE-mediated translational control', *Cell* 132(3): 434-48.

Rao, R. V. and Bredesen, D. E. (2004) 'Misfolded proteins, endoplasmic reticulum stress and neurodegeneration', *Curr Opin Cell Biol* 16(6): 653-62.

Richter, J. D. and Lasko, P. (2011) 'Translational control in oocyte development', *Cold Spring Harb Perspect Biol* 3(9): a002758.

Sasikumar, Arjun N., Perez, Winder B. and Kinzy, Terri Goss (2012) 'The many roles of the eukaryotic elongation factor 1 complex', *Wiley Interdisciplinary Reviews: RNA* 3(4): 543-555.

Schagger, H. (2006) 'Tricine-SDS-PAGE', *Nat Protoc* 1(1): 16-22.

Schroder, M. and Kaufman, R. J. (2005) 'ER stress and the unfolded protein response', *Mutat Res* 569(1-2): 29-63.

Selman, K., Wallace, R. A., Sarka, A. and Qi, X. (1993) 'Stages of oocyte development in the zebrafish, Brachydanio rerio', *J Morphol* 218(2): 203-224.

Shen, X., Zhang, K. and Kaufman, R. J. (2004) 'The unfolded protein response--a stress signaling pathway of the endoplasmic reticulum', *J Chem Neuroanat* 28(1-2): 79-92.

Shen, Xiaohua, Ellis, Ronald E., Lee, Kyungho, Liu, Chuan-Yin, Yang, Kun, Solomon, Aaron, Yoshida, Hiderou, Morimoto, Rick, Kurnit, David M., Mori, Kazutoshi et al. (2001) 'Complementary Signaling Pathways Regulate the Unfolded Protein Response and Are Required for C. elegans Development', *Cell* 107(7): 893-903.

Silva, Jose, Nichols, Jennifer, Theunissen, Thorold W., Guo, Ge, van Oosten, Anouk L., Barrandon, Ornella, Wray, Jason, Yamanaka, Shinya, Chambers, Ian and Smith, Austin (2009) 'Nanog Is the Gateway to the Pluripotent Ground State', *Cell* 138(4): 722-737.

Smibert, C. A., Lie, Y. S., Shillinglaw, W., Henzel, W. J. and Macdonald, P. M. (1999) 'Smaug, a novel and conserved protein, contributes to repression of nanos mRNA translation in vitro', *RNA* 5(12): 1535-47.

Smibert, C. A., Wilson, J. E., Kerr, K. and Macdonald, P. M. (1996) 'smaug protein represses translation of unlocalized nanos mRNA in the Drosophila embryo', *Genes Dev* 10(20): 2600-9.

Snee, M., Benz, D., Jen, J. and Macdonald, P. M. (2008) 'Two distinct domains of Bruno bind specifically to the oskar mRNA', *RNA Biol* 5(1): 1-9.

Sun, J., Yan, L., Shen, W. and Meng, A. (2018) 'Maternal Ybx1 safeguards zebrafish oocyte maturation and maternal-to-zygotic transition by repressing global translation', *Development* 145(19).

Takahashi, Kazutoshi and Yamanaka, Shinya (2006) 'Induction of Pluripotent Stem Cells from Mouse Embryonic and Adult Fibroblast Cultures by Defined Factors', *Cell* 126: 663-676.

Thisse, C. and Thisse, B. (2008) 'High-resolution in situ hybridization to whole-mount zebrafish embryos', *Nat Protoc* 3(1): 59-69.

Trapnell, C., Williams, B. A., Pertea, G., Mortazavi, A., Kwan, G., van Baren, M. J., Salzberg, S. L., Wold, B. J. and Pachter, L. (2010) 'Transcript assembly and quantification by RNA-Seq reveals unannotated transcripts and isoform switching dur ing cell differentiation', *Nat Biotechnol* 28(5): 511-5.

Veil, M., Schaechtle, M. A., Gao, M. J., Kirner, V., Buryanova, L., Grethen, R. and Onichtchouk, D. (2018) 'Maternal Nanog is required for zebrafish embryo architecture and for cell viability during gastrulation', *Development* 145(1).

Veil, M., Yampolsky, L. Y., Gruning, B. and Onichtchouk, D. (2019) 'Pou5f3, SoxB1, and Nanog remodel chromatin on high nucleosome affinity regions at zygotic genome activation', *Genome Res*.

Wang, M., Ly, M., Lugowski, A., Laver, J. D., Lipshitz, H. D., Smibert, C. A. and Rissland, O. S. (2017) 'ME31B globally represses maternal mRNAs by two distinct mechanisms during

the Drosophila maternal-to-zygotic transition', *Elife* 6.

Wei, C. Y., Wang, H. P., Zhu, Z. Y. and Sun, Y. H. (2014) 'Transcriptional factors smad1 and smad9 act redundantly to mediate zebrafish ventral specification downstream of smad5', *J Biol Chem* 289(10): 6604-6618.

Westerfield, Monte. (1995) *The zebrafish book : a guide for the laboratory use of zebrafish (Danio rerio)*, Eugene, OR: M. Westerfield.

Winata, Cecilia Lanny, Łapiński, Maciej, Pryszcz, Leszek, Vaz, Candida, bin Ismail, Muhammad Hisyam, Nama, Srikanth, Hajan, Hajira Shreen, Lee, Serene Gek Ping, Korzh, Vladimir, Sampath, Prabha et al. (2017) 'Cytoplasmic polyadenylation-mediated translational control of maternal mRNAs directs maternal to zygotic transition', *Development*.

Xu, C., Fan, Z. P., Muller, P., Fogley, R., DiBiase, A., Trompouki, E., Unternaehrer, J., Xiong, F., Torregroza, I., Evans, T. et al. (2012) 'Nanog-like regulates endoderm formation through the Mxtx2-Nodal pathway', *Developmental Cell* 22(3): 625-38.

Yarunin, A., Harris, R. E., Ashe, M. P. and Ashe, H. L. (2011) 'Patterning of the Drosophila oocyte by a sequential translation repression program involving the d4EHP and Belle translational repressors', *RNA Biol* 8(5): 904-12.

Ye, D., Wang, X., Wei, C., He, M., Wang, H., Wang, Y., Zhu, Z. and Sun, Y. (2019) 'Marcksb plays a key role in the secretory pathway of zebrafish Bmp2b', *PLoS Genet* 15(9): e1008306.

Yoshida, Hiderou, Matsui, Toshie, Yamamoto, Akira, Okada, Tetsuya and Mori, Kazutoshi (2001) 'XBP1 mRNA Is Induced by ATF6 and Spliced by IRE1 in Response to ER Stress to Produce a Highly Active Transcription Factor', *Cell* 107(7): 881-891.

Zhang, F., Hao, Y., Li, X., Li, Y., Ye, D., Zhang, R., Wang, X., He, M., Wang, H., Zhu, Z. et al. (2021) 'Surrogate production of genome-edited sperm from a different subfamily by spermatogonial stem cell transplantation', *Sci China Life Sci*.

Zhang, Q., Ye, D., Wang, H., Wang, Y. and Sun, Y. (2020) 'Zebrafish cyp11c1 knockout reveals the roles of 11-ketotestosterone and cortisol in sexual development and reproduction', *Endocrinology*.

866

867 **Figure legend**

868 **Fig. 1. Loss of maternal *nanog* resulted in oocyte maturation defects.** (A)
869 Bright-field images showing the embryonic malformation of M*nanog* mutants in
870 contrast to time-matched WT embryos. Scale bar, 100μm. (B) WT and M*nanog*
871 embryos with chorions at 15 min post-fertilization (mpf). Scale bar, 100μm. (C,
872 D) Measurement of chorion diameter and oocyte diameter at 15 mpf.
873 ***P<0.001. N=20. (E) Representative images showing labelling of cortical
874 granules (CG) in WT and *nanog* mutant eggs fixed at 10 mpa. F-actin was
875 stained using phalloidin to show the outline of embryo. Scale bar, 100μm.
876 N=25. (F) Appearance of ovaries dissected from WT and *nanog*$^{-/-}$ females.
877 Scale bar, 1mm. (G) The GSI scatterplot of WT and *nanog*$^{-/-}$ females. N=8. GSI,
878 gonadosomatic index. *P<0.05. (H) Morphology of stage IV oocytes dissected
879 from WT and *nanog*$^{-/-}$ ovaries with incubation of
880 17α,20β-dihydroxy-4-pregnen-3-one (DHP, 1μg/mL) after 2 h. Scale bar, 1mm.
881 (I) Comparison of the %GVBD in WT and *nanog* mutant oocytes. 6 WT and 10
882 *nanog*$^{-/-}$ fishes were analyzed. (J) Stage V oocytes from WT and *nanog*
883 mutant. Insets show enlarged regions of the yolk and relative opaqueness is
884 seen in *nanog* mutants. Scale bar, 100μm. (K) SDS-PAGE and Coomassie
885 staining of major yolk proteins of stage III oocytes and stage V oocytes. The
886 higher and lower molecular weight yolk proteins (HYP and LYP) are indicated
887 by the red arrowhead. HYP/LYP ratios were calculated to represent yolk
888 protein cleavage levels.

Fig. 2. Loss of *nanog* triggers ER stress/unfolded protein response (UPR) and elevates global translation activity. (A) Fluorescent images showing mCherry reporter levels with GFP protein control levels in WT and M*nanog* embryos at 4hpf. Scale bar, 100μm. (B) Measurement of mCherry reporter intensities relative to GFP. ***P*<0.01. n=14. (C, D) Western blotting analysis of mCherry reporter levels at 4 hpf. **P*<0.05; Student's t-test. (E) Western blot analysis showed increased expression of Hspa5 (Bip) and Ddit3 (CHOP) in *nanog*$^{-/-}$ ovary. (F-I) RT-qPCR analysis of *hsp5a* (F), *ddit3* (G), *atf6* (H) and *ire1a* (I) in WT and *nanog*$^{-/-}$ ovaries. ***P*<0.01, ****P*<0.001. (J) Western blot analysis of S6 and phosphorylated S6 in WT and *nanog*$^{-/-}$ ovary. (K) statistical analysis of phosphorylated S6/S6 level in panel J. (L) Morphology of stage IV oocytes dissected from *nanog*$^{-/-}$ ovaries and treated with PERK inhibitor after 2h. Oocytes dissected from 3 fishes were treated for 2 hours in the presence of DHP. Final concentration: GSK2606414, 50 nM; ISRIB, 5 μM; DHP: 1μg/mL. Scale bar, 1mm. (M) %GVBD comparison in *nanog* mutant oocytes treated with or without PERK inhibitor. n=3. ***P*<0.01, ****P*<0.001.

Fig. 3. Nanog transcriptionally inhibits the expression of *eef1a1l2*. (A) RNA-seq analysis showed significantly increased expression of *eef1a1l2* in *nanog* null egg. Red dots indicate upregulated genes, green dots indicate down-regulated genes, and blue dots indicate no difference genes in *nanog*

mutant egg. (B) Upregulated expression of *eef1a1l2* in *nanog* mutant oocytes at different stages revealed by RT-qPCR. ***P*<0.01, ****P*<0.001. (C) In situ hybridization on cryosections of ovaries and WISH analysis of unfertilized eggs revealed increased expression of *eef1a1l2* in *nanog* mutant. Scale bar, 200μm. (D,E) WISH (D) and RT-qPCR (E) analysis showed reduced expression of *eef1a1l2* in *nanog* or En-*nanog* overexpressed embryos at 6 hpf. ***P*<0.01. Scale bar, 100μm. (F) ChIP analysis of *Tg*(CMV:*nanog-myc*) ovaries with anti-Myc antibody at 6mpf. The promoter region of *eef1a1l2* was enriched in precipitated chromatin. *rpl5*b was served as a negative control.

Fig. 4. Depletion of *eef1a1l2* rescues the impaired oocyte maturation of *nanog* mutant. (A) WT, M*nanog* and M*nanog*, M*eef1a1l2* embryos with chorions at 15 min post-fertilization (mpf). Scale bar, 100μm. (B,C) Measurement of chorion diameters and oocyte diameters at 15 mpf. **P*<0.05, ***P*<0.01, ****P*<0.001. n=20. (D) Representative images showing labelling of cortical granules (CG) in WT, *nanog*, and *nanog-eef1a1l2* double mutant eggs fixed at 10 mpa. F-actin was stained using phalloidin to show the outline of embryo. n=15. Scale bar, 100μm. (E) Appearance of ovaries dissected from WT, *nanog*$^{-/-}$ and *nanog*$^{-/-}$,*eef1a1l2*$^{-/-}$ females. Scale bar, 1mm. (F) The GSI scatterplot of WT, *nanog*$^{-/-}$ and *nanog*$^{-/-}$,*eef1a1l2*$^{-/-}$ females. n=3. GSI, gonadosomatic index. ***P*<0.01, ****P*<0.001. (G) Morphology of eggs from WT, *nanog*$^{-/-}$ and *nanog*$^{-/-}$,*eef1a1l2*$^{-/-}$. Insets show enlarged regions of the yolk.

Scale bar, 100μm. (H) SDS-PAGE and Coomassie staining of major yolk proteins of stage III oocytes and stage V eggs. The higher and lower molecular weight yolk proteins (HYP and LYP) are indicated by the arrow. HYP/LYP ratios were calculated to represent yolk protein cleavage levels. (I) Morphology of stage IV oocytes dissected from WT, *nanog*$^{-/-}$ and *nanog*$^{-/-}$,*eef1a1l2*$^{-/-}$ ovaries with incubation of DHP (1μg/mL) after 2h. Scale bar, 1mm. (J) Comparison of the %GVBD in WT, *nanog*$^{-/-}$ and *nanog*$^{-/-}$,*eef1a1l2*$^{-/-}$ oocytes. WT n=11, *nanog*$^{-/-}$ n=9, *nanog*$^{-/-}$,*eef1a1l2*$^{-/-}$ n=7.

Fig. 5. Depletion of *eef1a1l2* ameliorates ER stress and UPR of *nanog* mutant oocyte. (A-D) RT-qPCR analysis showed expression reduction of *hspa5* (A), *ddit3* (B), *atf6* (C) and *ire1a* (D) in *nanog* and *eef1a1l2* double mutant ovary, compared with *nanog* mutant ovary. **P*<0.05, ***P*<0.01, ****P*<0.001. (E, F) RT-PCR examination of *xbp1* splicing. The ratio of spliced *xbp1* (*xbp1s*) mRNA to unspliced *xbp1* (*xbp1u*) mRNA was increased in *nanog* mutant ovary, but restored in *nanog* and *eef1a1l2* double mutant. *gapdh* is used as internal control. The *xbp1s*/*xbp1u* ratio in F represents the intensity ratio of corresponding PCR product bands in E. (G) Observation of ER, Golgi and mitochondria structure in WT, *nanog* mutant and double mutant at stage I oocytes by transmission electron microscopy. White arrowheads indicate Golgi apparatus, yellow arrowheads indicate mitochondria, red arrowheads indicate lysosome. Scale bar, 0.5 μm.

Fig. 6. Maternal depletion of *eef1a1l2* rescues early embryonic defects of *nanog* mutant. (A) Phenotype of WT, M*nanog*, M*nanog*,M*eef1a1l2*, M*nanog*,MZ*eef1a1l2* and M*nanog*,Z*eef1a1l2,* embryos at 0.2, 8, 12, and 24 hpf. Scale bar, 100 μm. (B) Detection of *mxtx2*, *mir-430* precursor, *blf* and *sod1* in WT, M*nanog* and M*nanog*,M*eef1a1l2* embryos by WISH at indicated stage. scale bar, 100 μm. (C) The model of Nanog function in oocyte and early embryo of zebrafish. Top: Nanog acts as a transcriptional repressor to suppress the expression of *eef1a1l2* and maintain the correct translation level of maternal mRNAs during oocyte development. Then Nanog switches to a transcriptional activator to prime zygotic genome activation in zygotes. Bottom: in WT oocyte, Nanog inhibits the transcription of *eef1a1l2* and maintain the proper level of global translation, ensuring appropriate amounts of proteins. Good egg quality and normal embryonic development is thus guaranteed. In the absence of maternal *nanog* (*nanog*$^{-/-}$), the balance of global translation is destroyed. Elevated translation resulted in excessive protein loading, further leads to poor egg quality and failure embryogenesis. In *nanog* and *eef1a1l2* double mutant oocyte (*nanog*$^{-/-,}$ *eef1a1l2*$^{-/-}$), global translation level is mitigated due to the absent of eEF1A1l2, protein overloading is relieved and egg quality is also improved, thereby promotes a better embryonic morphology formation.

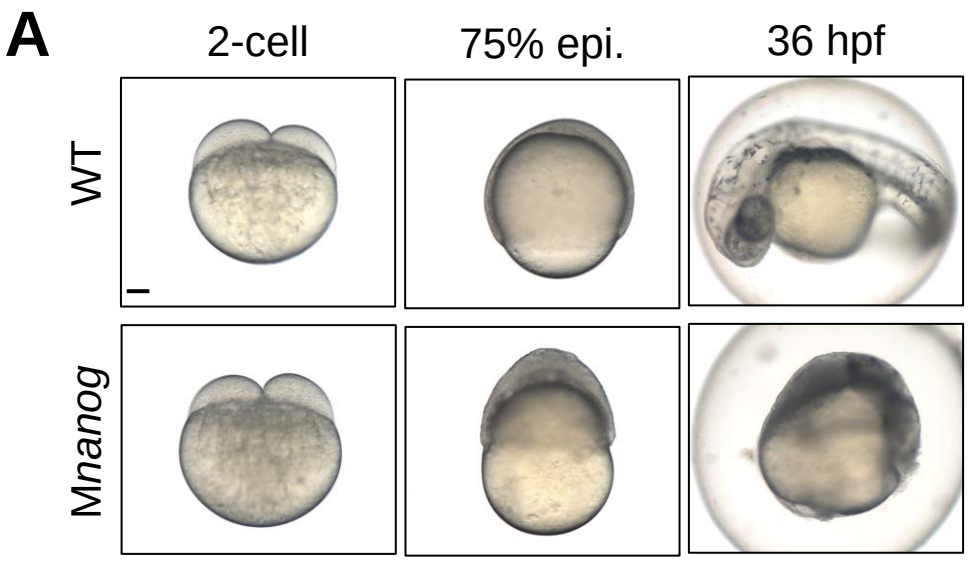

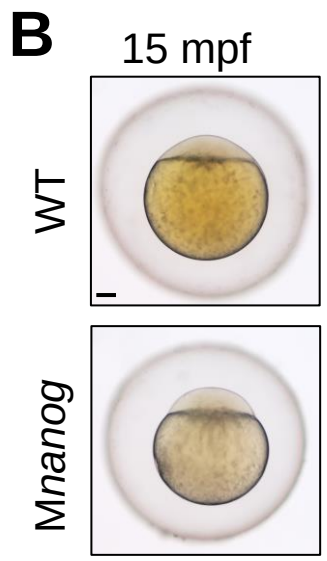

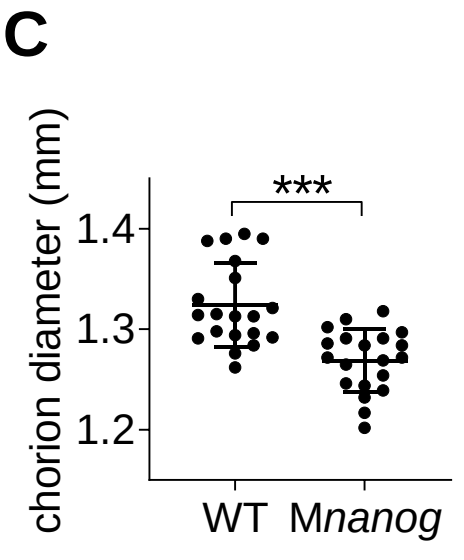

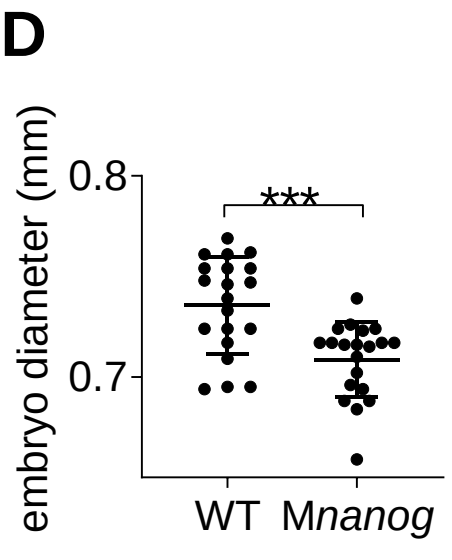

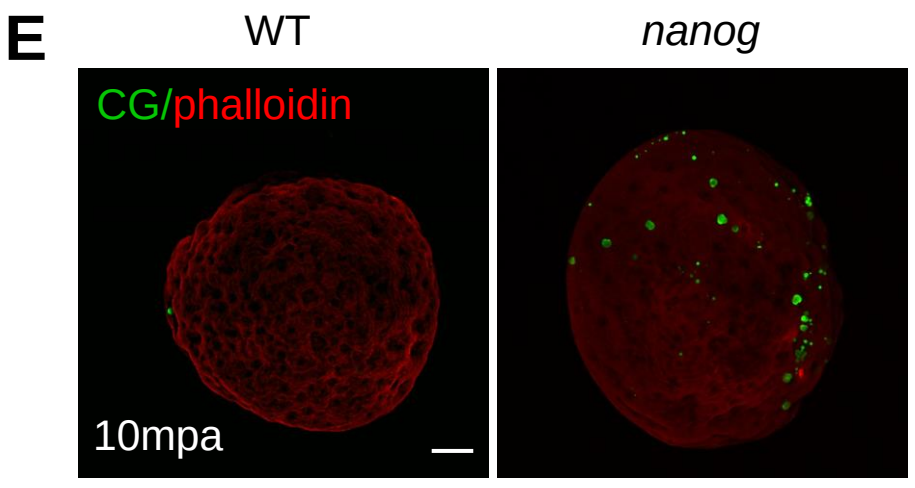

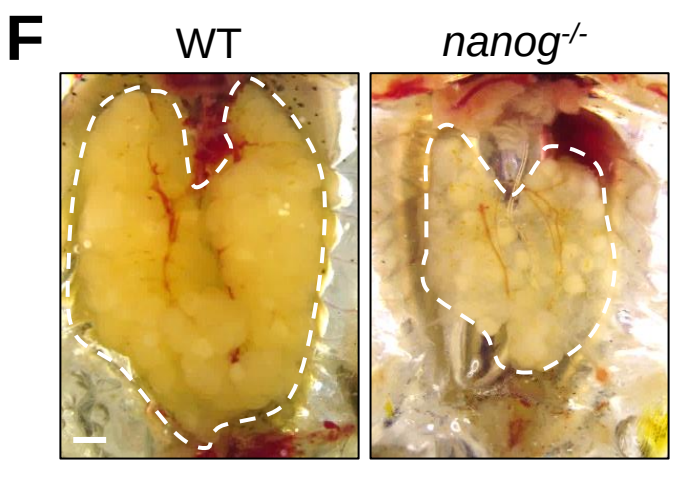

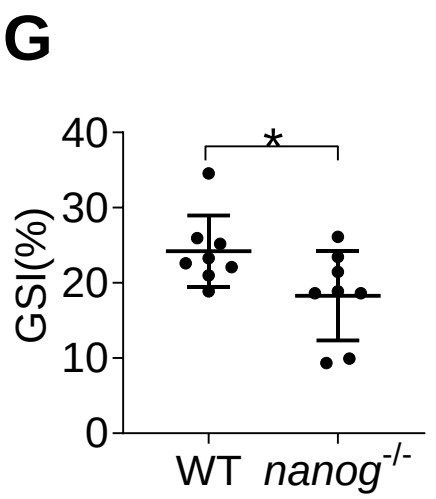

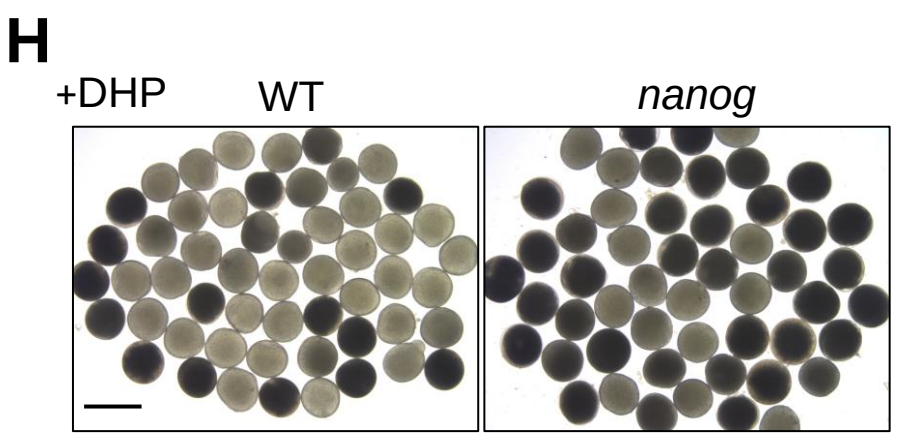

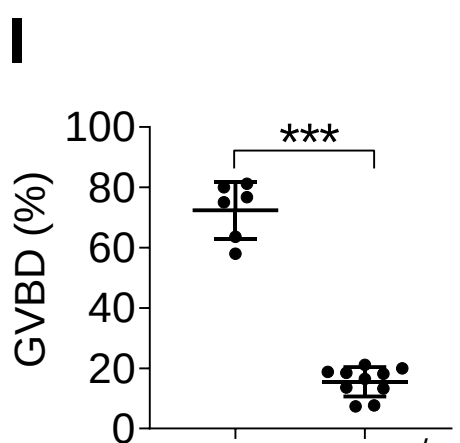

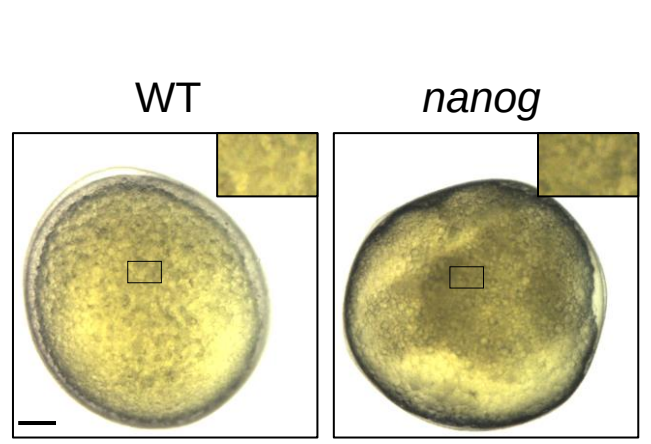

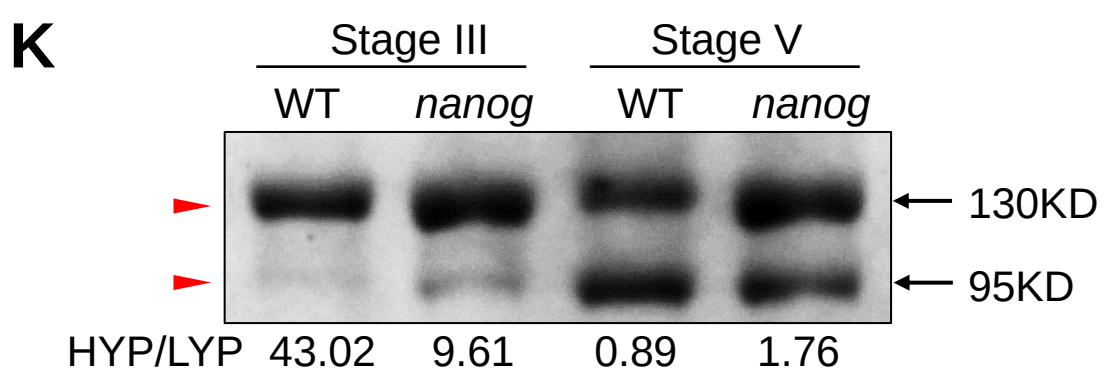

He et al., Fig. 1

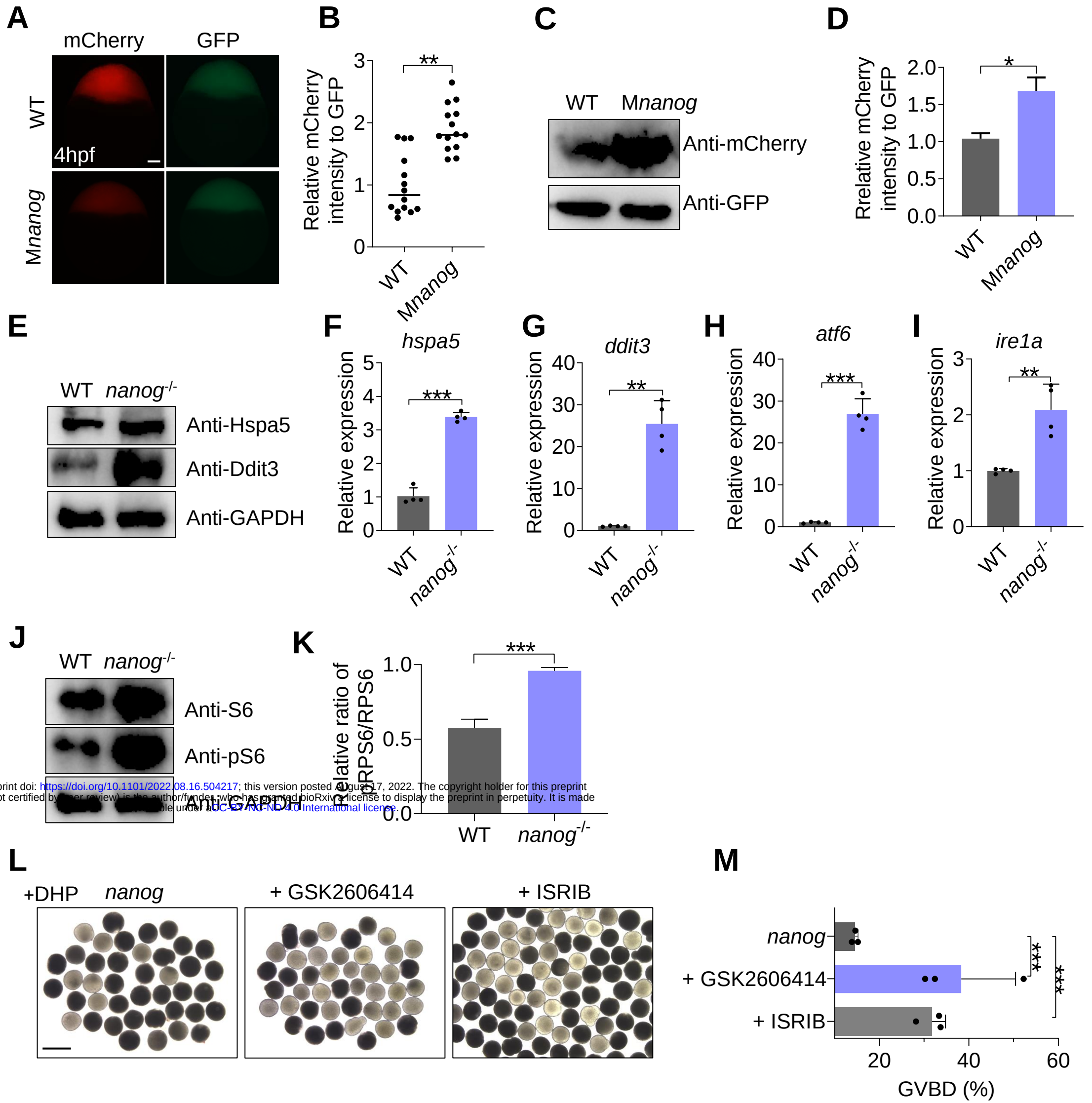

He et al., Fig. 2

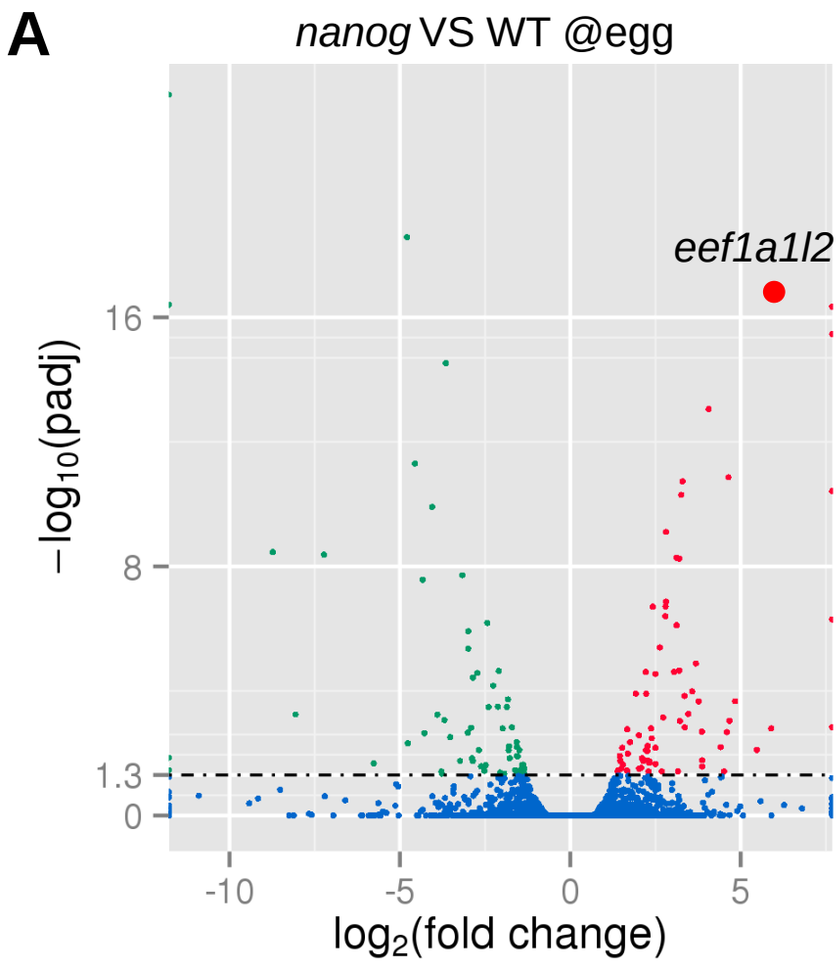

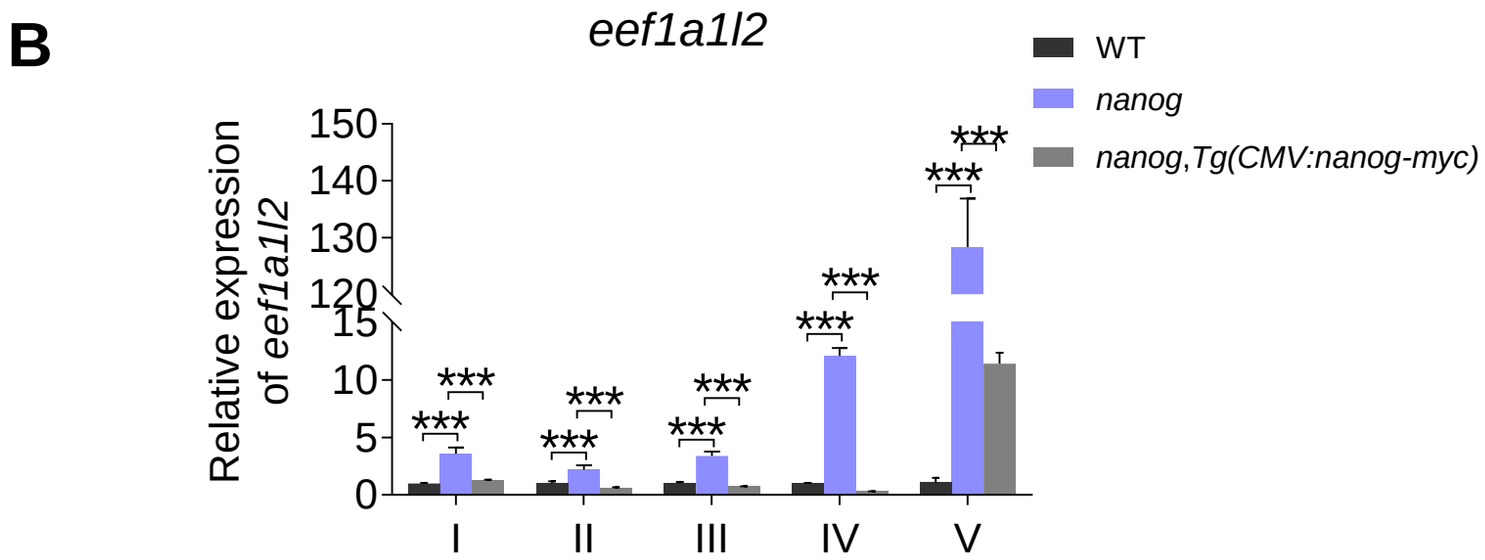

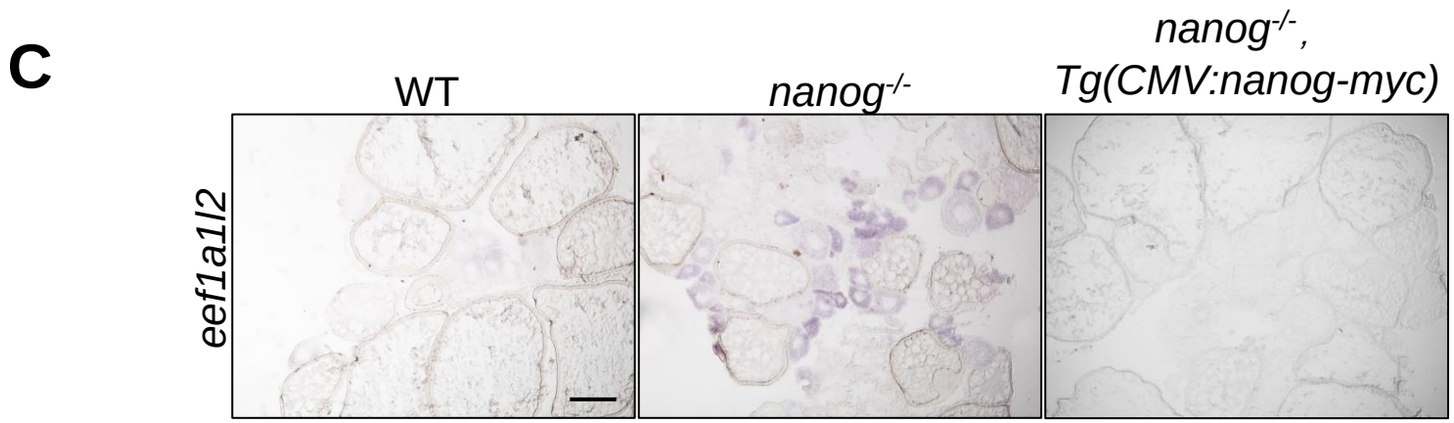

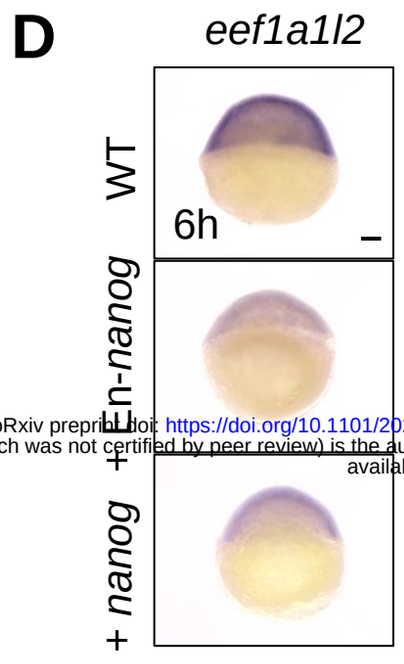

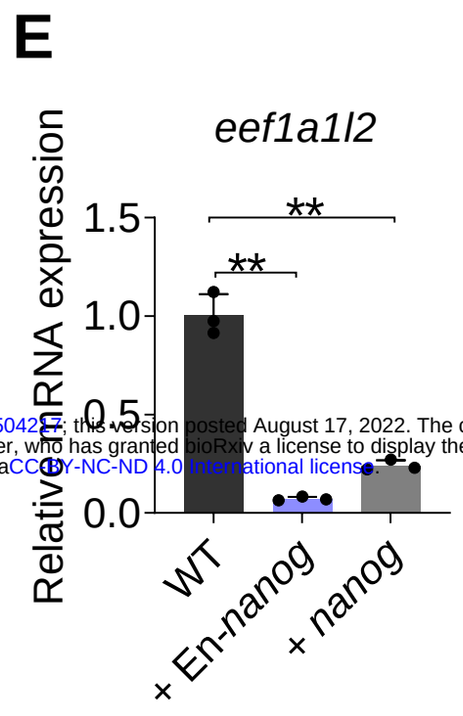

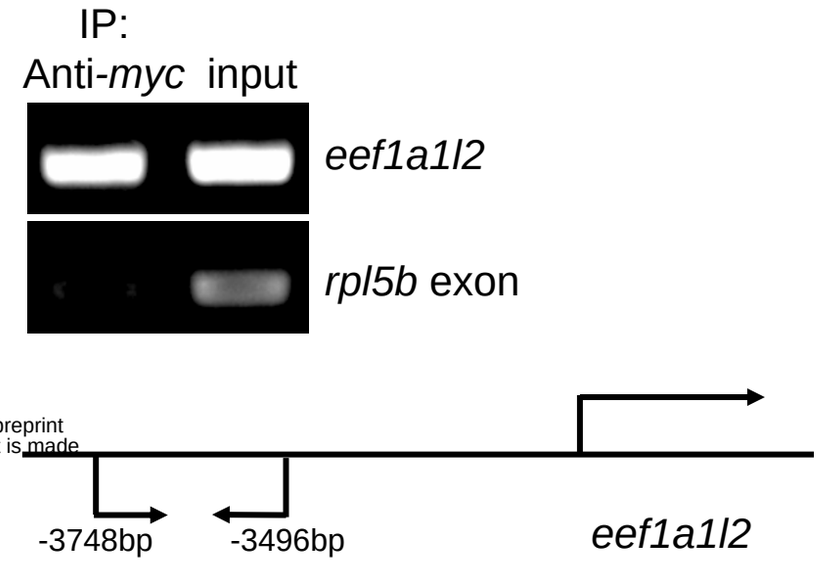

He et al., Fig. 3

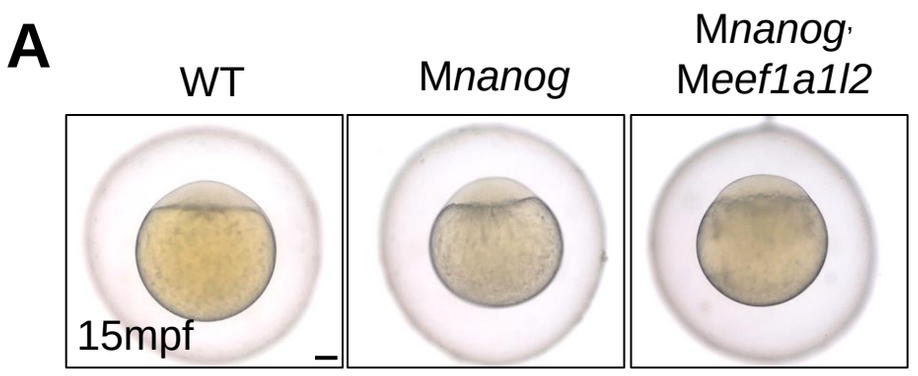

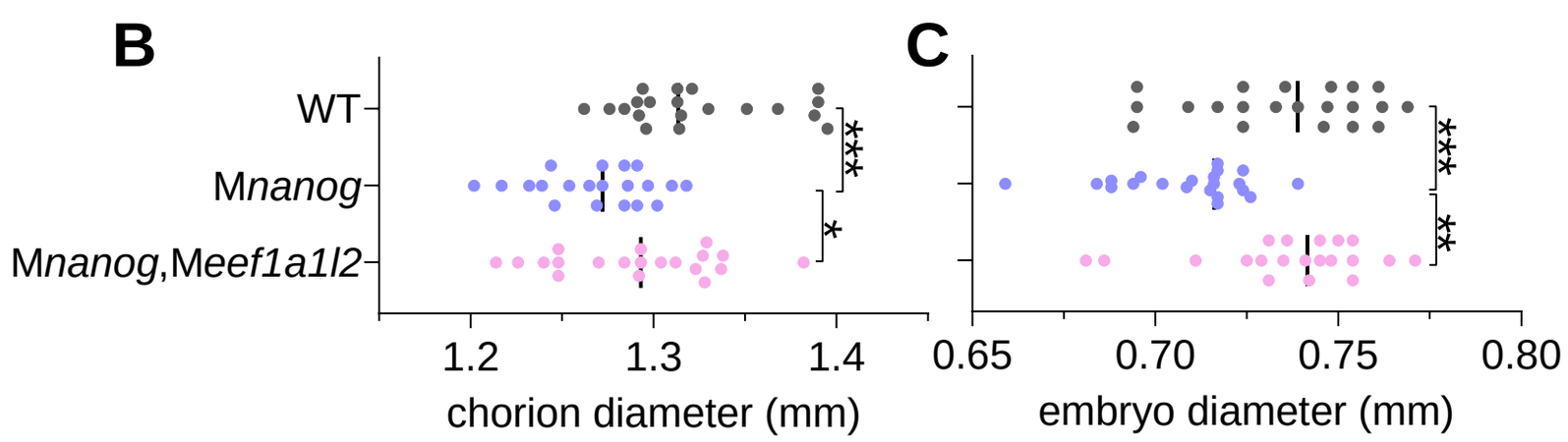

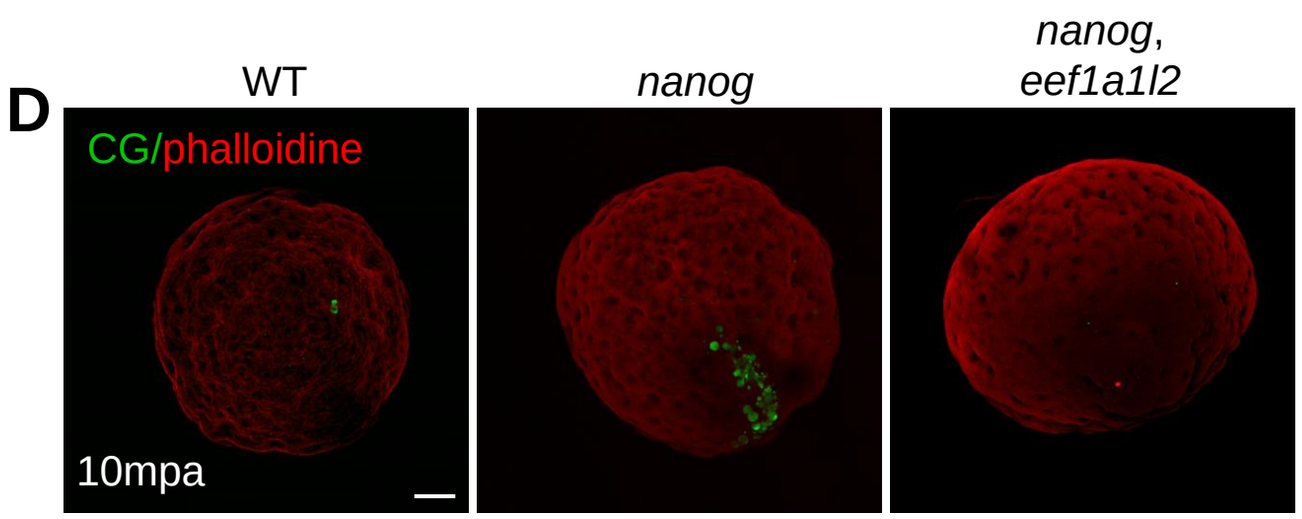

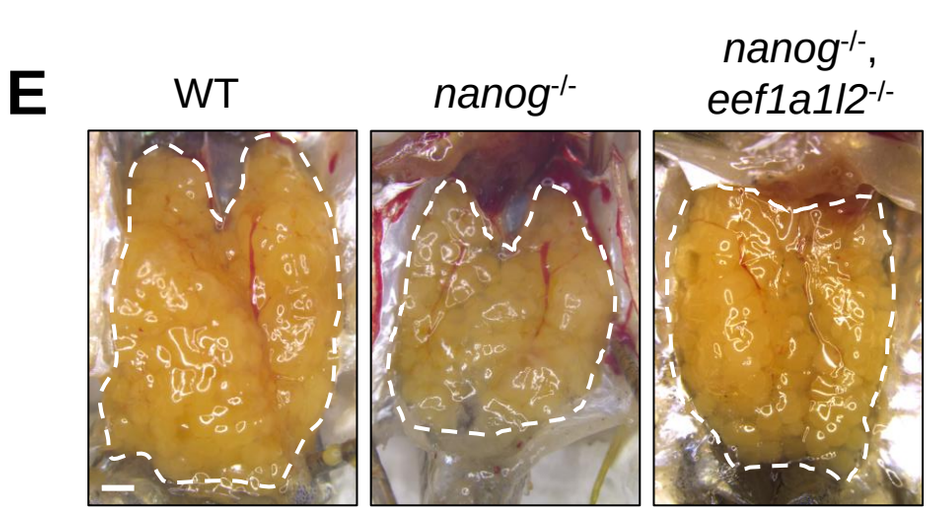

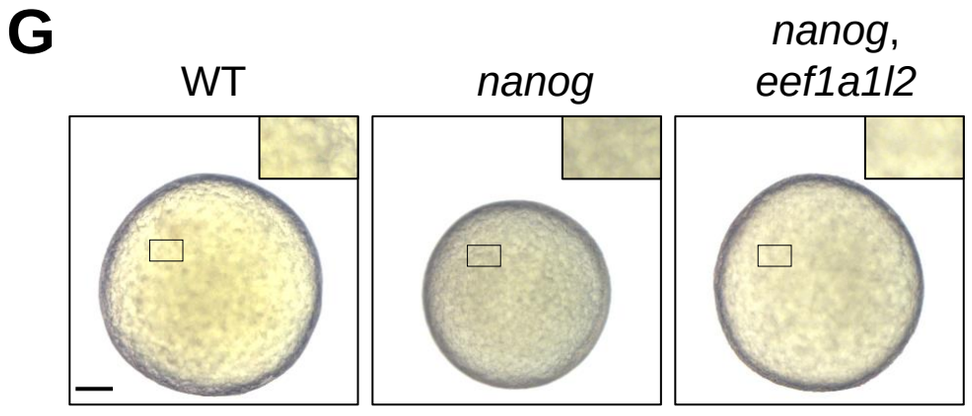

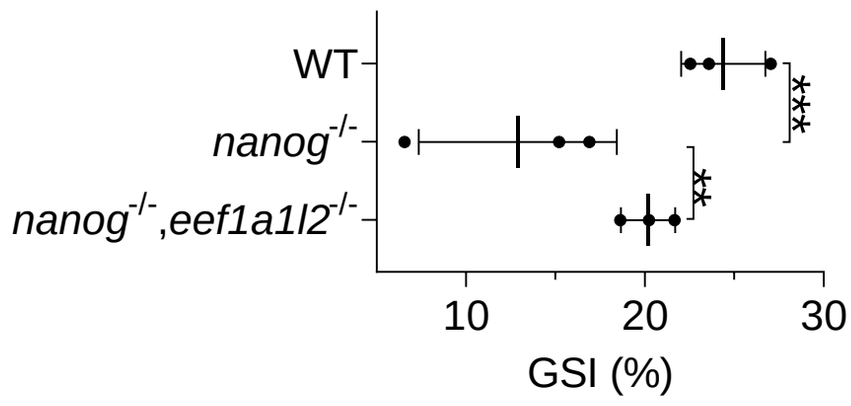

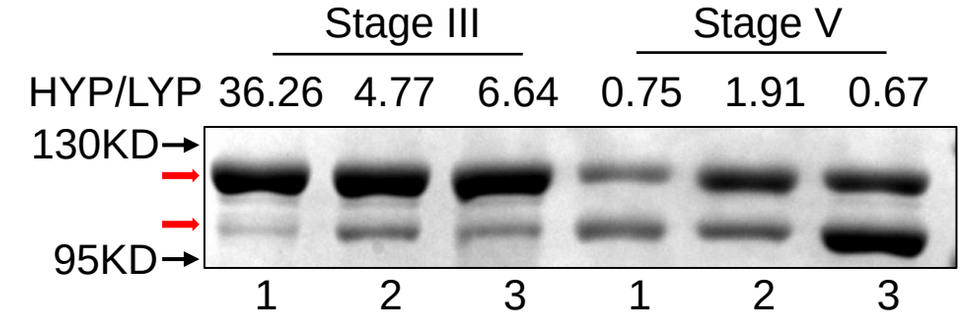

1: WT;
2: *nanog*
3: *nanog*,*eef1a1l2*

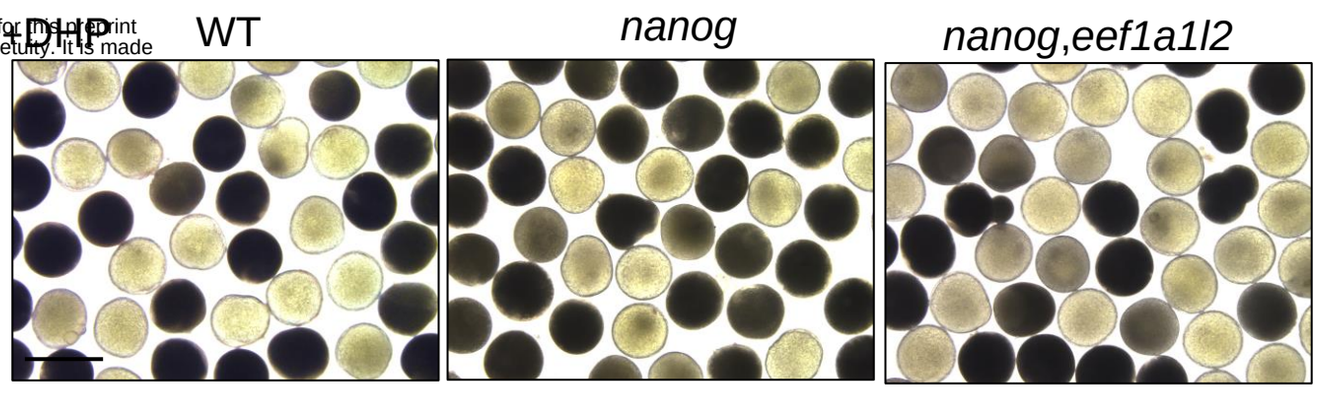

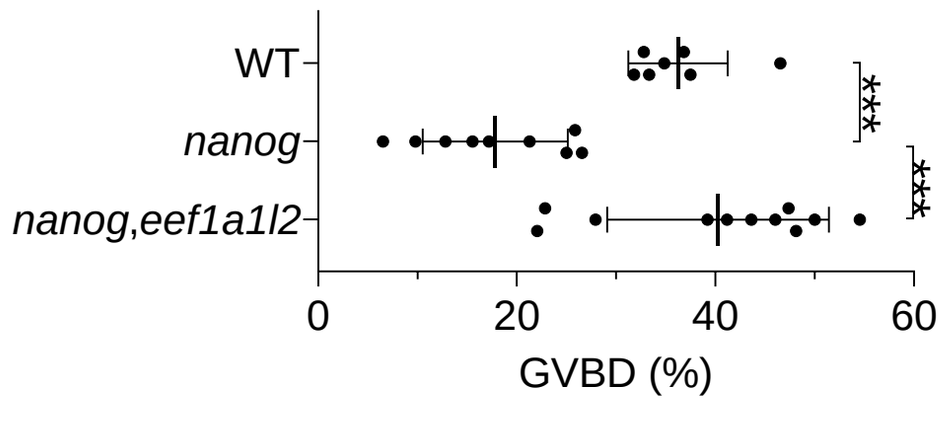

He et al., Fig. 4

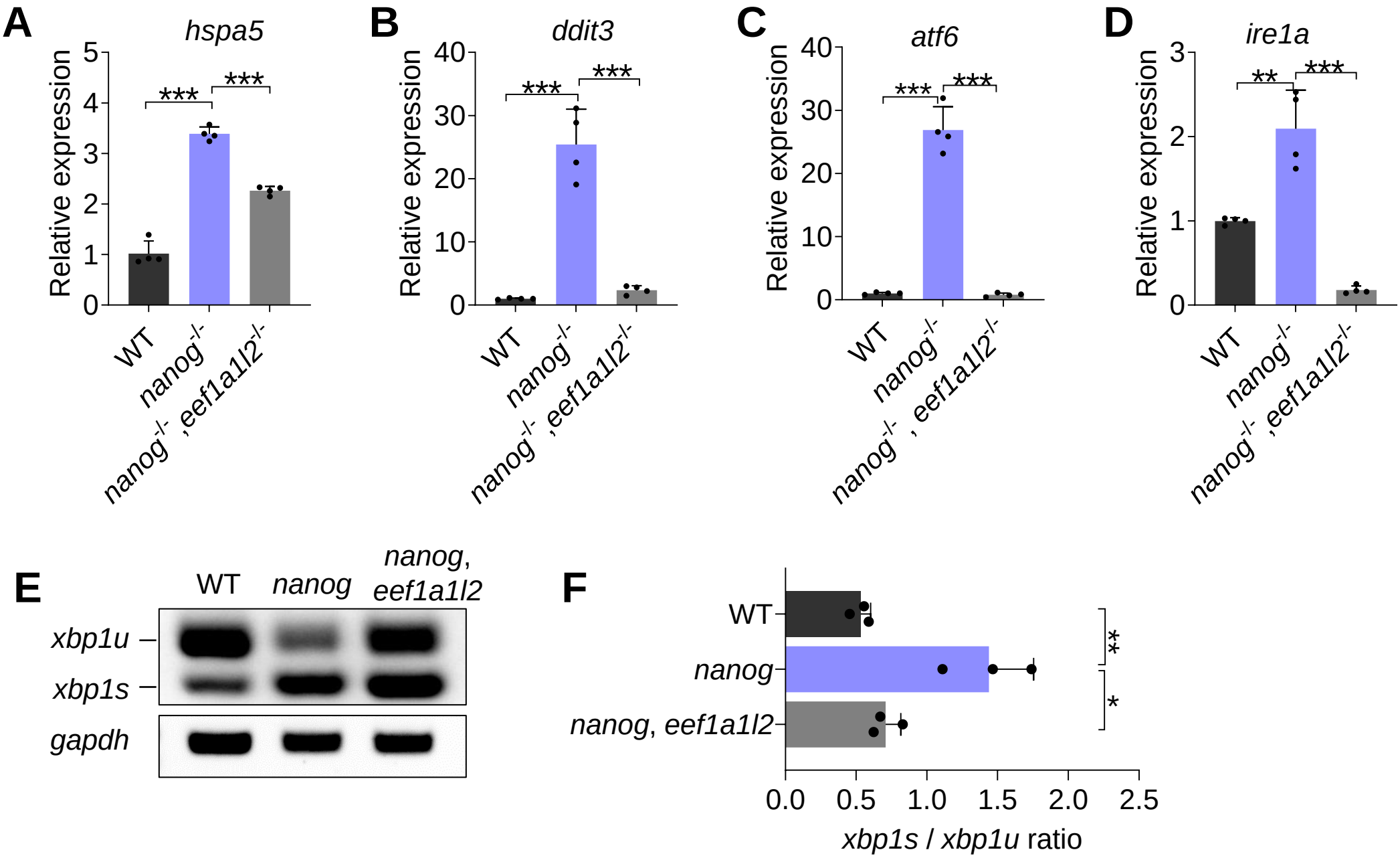

He et al., Fig. 5

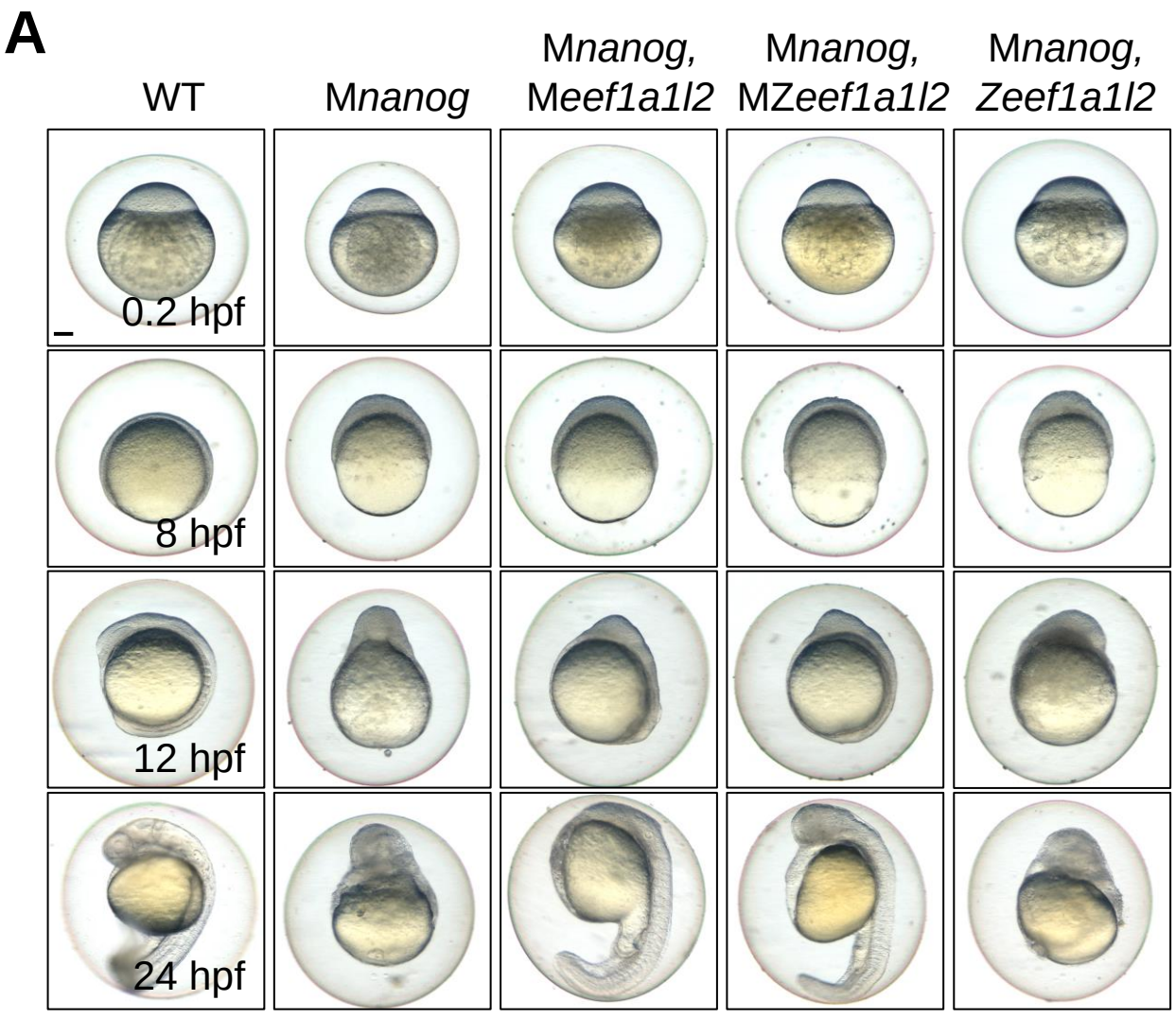

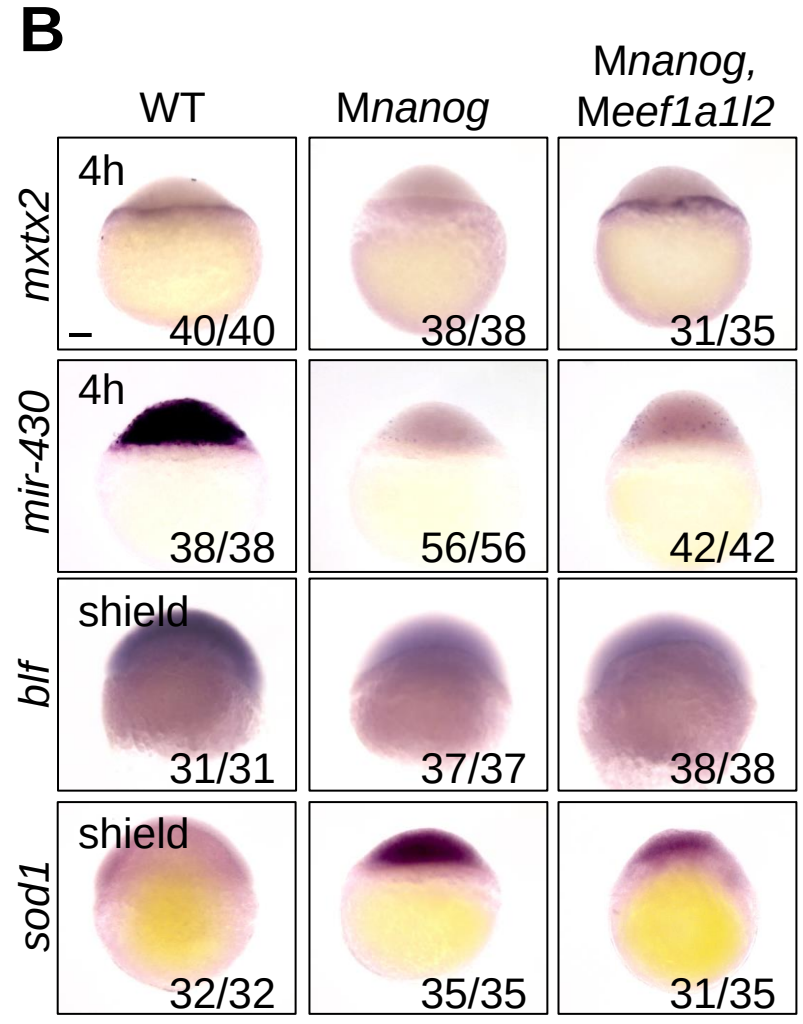

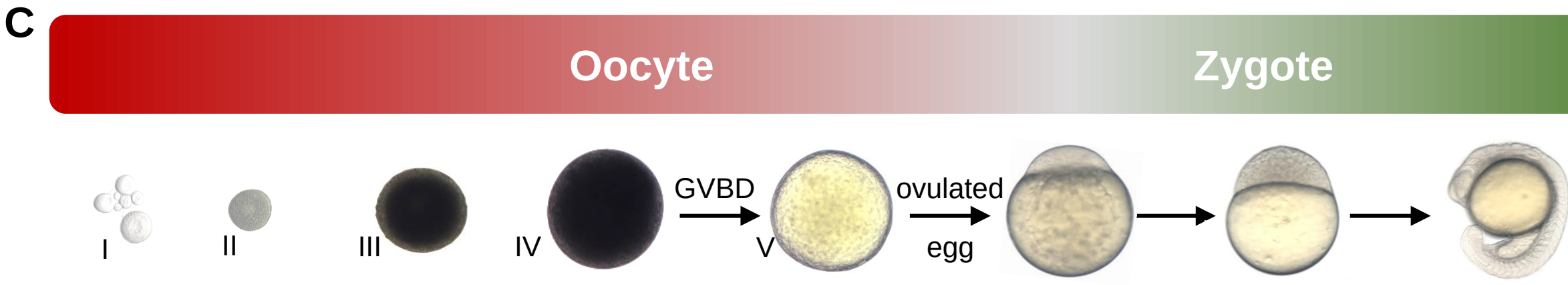

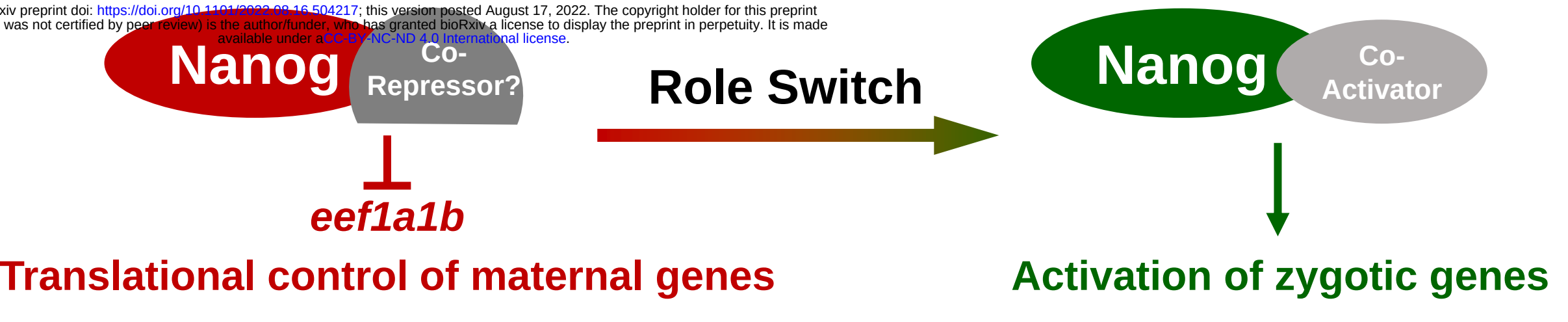

He et al., Fig. 6